30. Garcia CC, Blair HJ, Seager M, Coulthard A, Tennant S, Buddles M, Curtis A, Goodship JA. Identification of a mutation in synapsin I, a synaptic vesicle protein, in a family with epilepsy. J Med Genet 2004;41:183–186. [PubMed: 14985377]
31. Toonen RF, Wierda K, Sons MS, de Wit H, Cornelisse LN, Brussaard A, Plomp JJ, Verhage M. Munc18-1 expression levels control synapse recovery by regulating readily releasable pool size. Proc Natl Acad Sci U S A 2006;103:18332–18337. [PubMed: 17110441]
32. Kitamura K, Yanazawa M, Sugiyama N, Miura H, Iizuka-Kogo A, Kusaka M, Omichi K, Suzuki R, Kato-Fukui Y, Kamiirisa K, Matsuo M, Kamijo S, Kasahara M, Yoshioka H, Ogata T, Fukuda T, Kondo I, Kato M, Dobyns WB, Yokoyama M, Morohashi K. Mutation of ARX causes abnormal development of forebrain and testes in mice and X-linked lissencephaly with abnormal genitalia in humans. Nat Genet 2002;32:359–369. [PubMed: 12379852]
33. Bonneau D, Toutain A, Laquerriere A, Marret S, Saugier-Veber P, Barthez MA, Radi S, Biran-Mucignat V, Rodriguez D, Gelot A. X-linked lissencephaly with absent corpus callosum and ambiguous genitalia (XLAG): clinical, magnetic resonance imaging, and neuropathological findings. Ann Neurol 2002;51:340–349. [PubMed: 11891829]
34. Kato M. A new paradigm for West syndrome based on molecular and cell biology. Epilepsy Res 2006;70(Suppl 1):S87–95. [PubMed: 16806828]
35. Kato M, Dobyns WB. X-linked lissencephaly with abnormal genitalia as a tangential migration disorder causing intractable epilepsy: proposal for a new term, "interneuronopathy". J Child Neurol 2005;20:392–397. [PubMed: 15921244]
36. Hamdan FF, Piton A, Gauthier J, Lortie A, Dubeau F, Dobrzeniecka S, Spiegelman D, Noreau A, Pellerin S, Cote M, Henrion E, Fombonne E, Mottron L, Marineau C, Drapeau P, Lafreniere RG, Lacaille JC, Rouleau GA, Michaud JL. De novo STXBP1 mutations in mental retardation and nonsyndromic epilepsy. Ann Neurol 2009;65:748–753. [PubMed: 19557857]
37. Guilmatre A, Dubourg C, Mosca AL, Legallic S, Goldenberg A, Drouin-Garraud V, Layet V, Rosier A, Briault S, Bonnet-Brilhault F, Laumonnier F, Odent S, Le Vacon G, Joly-Helas G, David V, Bendavid C, Pinoit JM, Henry C, Impallomeni C, Germano E, Tortorella G, Di Rosa G, Barthelemy C, Andres C, Faivre L, Frebourg T, Saugier Veber P, Campion D. Recurrent rearrangements in synaptic and neurodevelopmental genes and shared biologic pathways in schizophrenia, autism, and mental retardation. Arch Gen Psychiatry 2009;66:947–956. [PubMed: 19736351]
38. Ramocki MB, Zoghbi HY. Failure of neuronal homeostasis results in common neuropsychiatric phenotypes. Nature 2008;455:912–918. [PubMed: 18923513]

REPORT

Identification of *KLHL41* Mutations Implicates BTB-Kelch-Mediated Ubiquitination as an Alternate Pathway to Myofibrillar Disruption in Nemaline Myopathy

Vandana A. Gupta,[1] Gianina Ravenscroft,[2] Ranad Shaheen,[3] Emily J. Todd,[2] Lindsay C. Swanson,[1] Masaaki Shiina,[4] Kazuhiro Ogata,[4] Cynthia Hsu,[1] Nigel F. Clarke,[5] Basil T. Darras,[6] Michelle A. Farrar,[7] Amal Hashem,[3] Nicholas D. Manton,[8] Francesco Muntoni,[9] Kathryn N. North,[10] Sarah A. Sandaradura,[5] Ichizo Nishino,[11] Yukiko K. Hayashi,[11] Caroline A. Sewry,[9] Elizabeth M. Thompson,[12,13] Kyle S. Yau,[2] Catherine A. Brownstein,[1] Timothy W. Yu,[1] Richard J.N. Allcock,[14] Mark R. Davis,[15] Carina Wallgren-Pettersson,[16] Naomichi Matsumoto,[17] Fowzan S. Alkuraya,[3] Nigel G. Laing,[2] and Alan H. Beggs[1,*]

Nemaline myopathy (NM) is a rare congenital muscle disorder primarily affecting skeletal muscles that results in neonatal death in severe cases as a result of associated respiratory insufficiency. NM is thought to be a disease of sarcomeric thin filaments as six of eight known genes whose mutation can cause NM encode components of that structure, however, recent discoveries of mutations in non-thin filament genes has called this model in question. We performed whole-exome sequencing and have identified recessive small deletions and missense changes in the Kelch-like family member 41 gene (*KLHL41*) in four individuals from unrelated NM families. Sanger sequencing of 116 unrelated individuals with NM identified compound heterozygous changes in *KLHL41* in a fifth family. Mutations in *KLHL41* showed a clear phenotype-genotype correlation: Frameshift mutations resulted in severe phenotypes with neonatal death, whereas missense changes resulted in impaired motor function with survival into late childhood and/or early adulthood. Functional studies in zebrafish showed that loss of Klhl41 results in highly diminished motor function and myofibrillar disorganization, with nemaline body formation, the pathological hallmark of NM. These studies expand the genetic heterogeneity of NM and implicate a critical role of BTB-Kelch family members in maintenance of sarcomeric integrity in NM.

Nemaline myopathy (NM) is a rare congenital disorder primarily affecting skeletal muscle function. Clinically, NM is a heterogeneous group of myopathies of variable severity.[1,2] The "severe" congenital form of NM presents with reduced or absent spontaneous movements in utero leading to severe contractures or fractures at birth and respiratory insufficiency leading to early mortality. Individuals with the "intermediate" congenital form of NM have antigravity movement and independent respiration at delivery but exhibit delayed motor milestones and require ventilatory support later in life. The "typical" congenital form of NM usually presents in the neonatal period or first year of life with hypotonia, weakness, and feeding difficulties with less prominent respiratory involvement. In these cases, the disease is usually static or very slowly progressive, and many individuals remain ambulant for much of their lives.[3] The defining diagnostic feature of all forms of NM, irrespective of genetic mutation, is the presence of numerous red-staining rods with Gomori trichrome stain that appear as rod-shaped electron-dense structures termed "nemaline bodies" by electron microscopy.[4] These nemaline bodies are most frequently cytoplasmic; however, the presence of intranuclear rods has also been reported.[5]

NM is a genetically heterogeneous condition, and mutations in eight different genes have been identified that are associated with dominant and/or recessive forms of this disease.[6–13] Mutations in these genes cause about 75%–80% of NM cases, suggesting the involvement of additional unidentified genes in disease etiology.

[1]Division of Genetics and Genomics, The Manton Center for Orphan Disease Research, Boston Children's Hospital, Harvard Medical School, Boston, MA 02115, USA; [2]Western Australian Institute for Medical Research and the Centre for Medical Research, University of Western Australia, Nedlands, Western Australia 6009, Australia; [3]Developmental Genetics Unit, King Faisal Specialist Hospital and Research Center, Riyadh 11211, Saudi Arabia; [4]Department of Biochemistry, Yokohama City University, Graduate School of Medicine, 3-9 Fukuura, Kanazawa-ku, Yokohama 236-0004, Japan; [5]Institute for Neuroscience and Muscle Research, Children's Hospital at Westmead and Discipline of Paediatrics and Child Health, University of Sydney, Sydney 2145, Australia; [6]Department of Neurology, Boston Children's Hospital, Harvard Medical School, Boston, MA 02115, USA; [7]Department of Neurology, Sydney Children's Hospital, Randwick NSW 2032, Australia; [8]Department of Surgical Pathology, SA Pathology at the Women's and Children's Hospital, North Adelaide, South Australia 5006; [9]Dubowitz Neuromuscular Centre, Institute of Child Health and Great Ormond Street Hospital, London WC1N 1EH, UK; [10]Murdoch Childrens Research Institute, The Royal Children's Hospital, Parkville, Victoria 3052, Australia; [11]Department of Neuromuscular Research, National Institute of Neuroscience, National Center of Neurology and Psychiatry, Tokyo 187-8502, Japan; [12]Department of Paediatrics, University of Adelaide, Adelaide, South Australia 5000, Australia; [13]SA Clinical Genetics Service, SA Pathology at the Women's and Children's Hospital, North Adelaide, South Australia 5006, Australia; [14]Lotterywest State Biomedical Facility Genomics and School of Pathology and Laboratory Medicine, University of Western Australia, Perth, Western Australia 6000, Australia; [15]Department of Anatomical Pathology, Royal Perth Hospital, Perth, Western Australia 6000, Australia; [16]The Folkhälsan Institute of Genetics, Samfundet Folkhälsan, Biomedicum Helsinki, PB 63 (Haartmaninkatu 8), and Department of Medical Genetics, Haartman Institute, University of Helsinki, Helsinki 00014, Finland; [17]Department of Human Genetics, Yokohama City University, Graduate School of Medicine, 3-9 Fukuura, Kanazawa-ku, Yokohama 236-0004, Japan
*Correspondence: beggs@enders.tch.harvard.edu
http://dx.doi.org/10.1016/j.ajhg.2013.10.020.

Therefore, we performed whole-exome sequencing (WES) combined, when applicable, with autozygome analysis to identify mutations in novel genes that underlie the disease pathology in a cohort of individuals affected with NM with unknown genetic diagnosis. All subjects were enrolled following informed consent and research was conducted according to the protocols approved by the Institutional Review Boards of the respective institutions in which these individuals were recruited. Molecular screening was performed on genomic DNA isolated from blood samples following standard protocols.

We performed whole-exome or whole-genome sequencing on a cohort of 60 unrelated NM probands through Boston Children's Hospital Gene Partnership facility. Molecular screening was performed on genomic DNA isolated from blood samples with standard protocols. Whole-blood DNA was subjected to solution capture (SureSelect Human All Exon V4, Agilent Technologies) to generate barcoded whole-exome sequencing libraries. Libraries were sequenced on an Illumina HiSeq 2000, employing paired end reads (100 bp × 2) to a mean target coverage of 96.5% and a mean read depth of 71.6. Alignment, variant calling, and annotation were performed with a custom informatics pipeline employing BWA,[14] Picard, and ANNOVAR[15] focusing on rare (<3% in db SNP135, 1000 Genomes Project Database, and the [EVS] National Heart, Lung, and Blood Institute Exome Sequencing Project Exome Variant Server) protein affecting changes in known and novel human disease genes. Alternatively, probands for families 203 and 832 were sequenced to greater than 50× depth by Axeq Technologies on an Illumina HiSeq 2000 following Agilent SureSelect Exome enrichment with their standard Exome Sequencing service. Whole-exome sequencing identified homozygous mutations of *KLHL41* in two unrelated families, suggesting this gene to be a candidate for NM. All *KLHL41* mutations are numbered relative to the mRNA sequence NM_006063.2 (where position 1 is the first base of the initiating MET codon) and protein NP_006054.2. Family 1 is a nonconsanguineous family of Vietnamese origin. Proband 203-1 is a 16-year-old female with an intermediate form of NM with a high-arched palate, dysarthria, and scoliosis who has required ventilatory support since childhood. WES identified an apparently homozygous c.103T>C transition in exon 1 resulting in a p.Cys35Arg substitution in this individual (Figure 1A). This variant was present as heterozygous in the father and absent in the mother. Copy number analysis in the affected region showed a heterozygous deletion in the mother and the proband, c.(?_-77)_(*602_?)del. Therefore, individual 203-1 is compound heterozygous for a deletion involving a portion of *KLHL41* and a KLHL41 p.Cys35Arg missense change. The second proband (832-1), who is adopted of Russian origin, is ambulant at age 12 and exhibits the typical congenital form of NM. WES identified a homozygous deletion of one base and an insertion of four bases c.459delinsACTC in the proband resulting in a single amino acid insertion, p.Ser153_Ala154insLeu in the protein (Figure 1A).

Whole-exome sequencing in probands with severe NM in Australian and Saudi Arabian cohorts resulted in identification of *KLHL41* mutations in two further families. The first (6462) is a consanguineous family of Persian origin from Afghanistan with one child (D12-203) affected with severe NM and four unaffected children (see Figure S1 available online). Homozygosity mapping was performed on the proband with the Illumina HumanCytoSNP-12 array, and the only known NM loci found within homozygous regions were *CFL2* (MIM 601443) and *NEB* (MIM 161650); however, both were excluded following Sanger sequencing, as was *ACTA1* (MIM 102610), which is the most common cause of simplex NM cases. WES of DNA from proband D12-203 was performed at the Lotterywest Sate Biomedical Facility Genomics Node, Royal Perth Hospital, Western Australia.[13] WES identified 453 heterozygous or homozygous variants. Application of the homozygosity data to the list of candidates reduced this to seven candidate variants. Two of these seven candidate variants were in skeletal-muscle-specific genes and of these the most likely candidate was a homozygous deletion within *KLHL41* (chr2: 170382132–170382139; c.1748_1755delAAGGAAAT, p.Lys583Thrfs*7) (Figure 1A). The deletion was confirmed by Sanger sequencing. Both parents and two unaffected siblings were heterozygous for the deletion, and two further unaffected siblings were homozygous for the normal allele.

Family 12DG1177, from a Saudi Arabian cohort is consanguineous (Figure S1). The male proband (12DG1177-1) was a newborn with severe hypotonia, dislocation of hips and knees, and facial dysmorphism in the form of micrognathia and cleft palate. There was a positive family history of two previous sibs who died of unknown causes soon after birth, as well as three healthy living sibs. The proband died of cardiorespiratory arrest shortly after intubation at less than 24 hr of age. Exome capture was performed with TruSeq Exome Enrichment kit (Illumina) as described earlier.[16] Only novel coding and splicing homozygous variants within the autozygome of the affected individual were considered. After filtering, 8,653 homozygous, coding, or splice variants were present, and autozygosity mapping, dbSNP, and analysis of 240 control Saudi exomes finally led to the identification of 18 candidate variants. The only truncating change was a single base deletion in *KLHL41* (c.641delA). This deletion was present in the coding region of exon 1 of *KLHL41* resulting in the frameshift change p.Asn214Thrfs*14 (Figure 1A).

Subsequent screening for *KLHL41* mutations in 116 individuals affected with severe, intermediate, or typical congenital forms of NM in the Boston and Australian NM Cohorts by Sanger sequencing identified a further family (D10-236) with compound heterozygous mutation (c.581_583delAAG, p.Glu194del and c.1238C>T, p.Ser413Leu) in proband. This individual is of Chinese

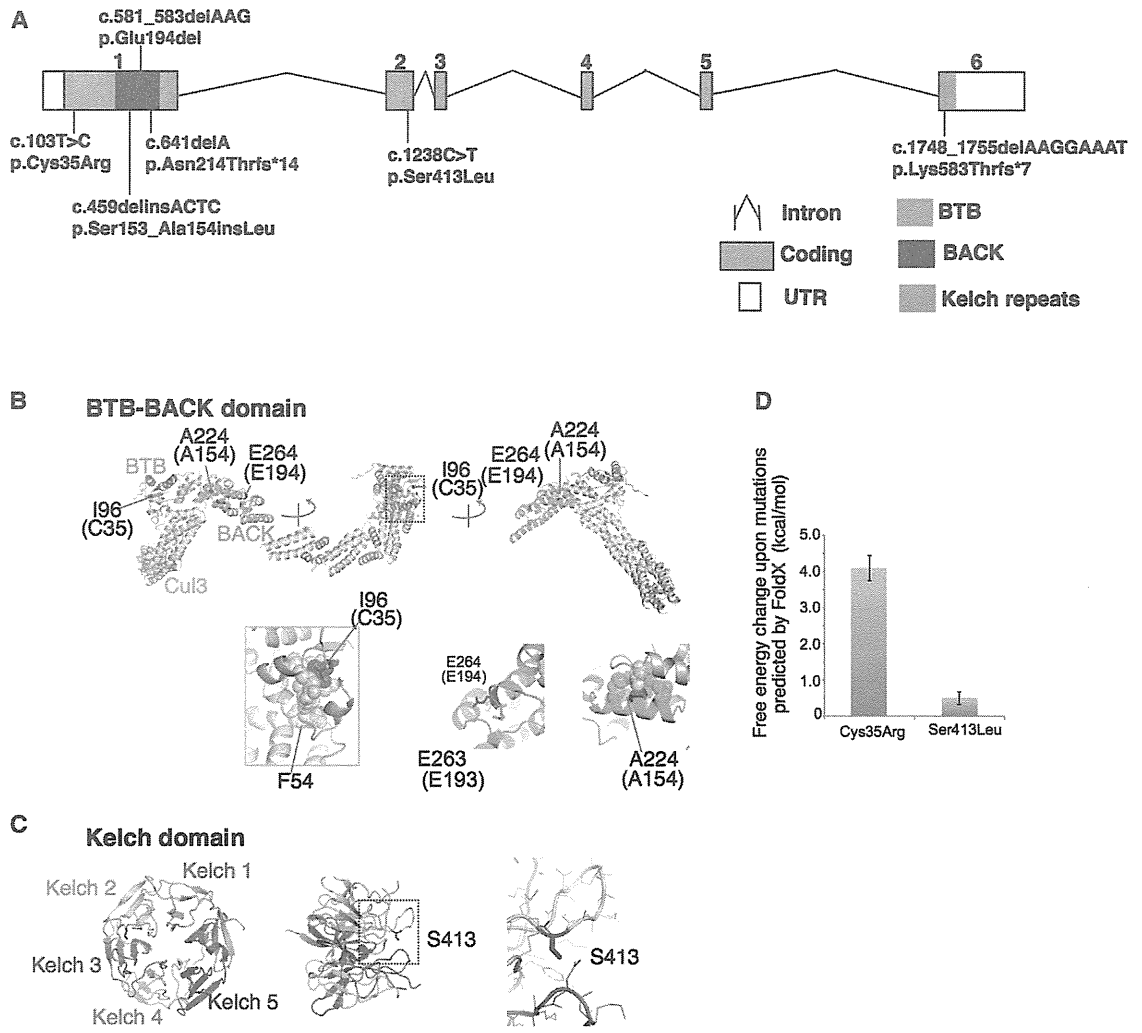

Figure 1. Overview of Mutations in *KLHL41* and Their Effect on Protein Structure

(A) Schematic representation of mutations in *KLHL41*. Boxes represent exons 1–6. Conserved domains of KLHL41 are indicated as follows: BTB (blue), BACK (red), and Kelch repeats (green). The BTB and BACK domains are encoded by exon 1 and the five Kelch repeats are encoded by exons 1–6.

(B and C) Crystal structures of the BTB-BACK domain of human Kelch-like protein (KLHL11) in complex with CUL3 (Protein Data Bank code 4AP2) (B) and the Kelch domain of rat KLHL41 (PDB code 2WOZ) (C). α helices, β strands, and loops are drawn as ribbons, arrows, and threads, respectively. The squared areas correspond to the close-up views in the insets. In (B), the BTB and BACK domains are colored pink and green, respectively, whereas CUL3 is colored yellow, except that Ile96, Ala224, and Glu264 (Cys35, Ala154, and Glu194 in human KLHL41, respectively) are colored red. The side chains of these residues and Glu263 (Glu193 in human KLHL41) are shown as sticks with the indications of amino acid numbers for human KLHL11 and those for human KLHL41 in parentheses. Side chains involved in hydrophobic cores around Ile96 and Ala224 are drawn in van der Waal's representation. In (C), the Kelch domain is color-coded to indicate each Kelch repeat, except that Ser413 is colored red. The side chain of Ser413 is shown as sticks. Molecular structures are drawn with PyMOL.

(D) Predicted free energy changes upon the substitutions of KLHL41 with FoldX software.

origin and exhibited the typical congenital form of NM. The detailed clinical features of affected individuals with mutations identified in *KLHL41* are presented in Table 1.

Overall, WES and Sanger sequencing resulted in identification of seven different mutations in Kelch-like family member 41 (*KLHL41*), previously known as *KBTBD10*, sarcosin, or *KRP1*, in affected NM individuals from five unrelated families (Figure 1A). Muscle histology was typical for NM: biopsies from probands of three different families (D12-203, 832-1, and 10-236) exhibited abnormal Gomori trichrome staining with presence of sarcoplasmic rods that varied from numerous small rods to fewer large rods in multiple myofibers (Figure 2A). No intranuclear rods or cores were seen. The missense changes identified in *KLHL41* are predicted to be pathogenic by polyphen, SIFT and pMUT and the mutated amino-acid residues are conserved in all representative species during evolution (Figure S2). The neighboring areas surrounding the sites of insertion or deletion are also relatively conserved, suggesting a structural or functional requirement for the altered amino acid residues (Figure S2). Sequencing of family members revealed that *KLHL41*

Table1. Clinical Manifestations in Affected Individuals Harboring *KLHL41* Mutations

Proband ID	cDNA Change	Amino Acid Change	Clinical Category	Sex	Nationality	Pregnancy and Delivery	Alive at Age/Mobility/ Age at Death	Associated Features
203-1	c.103T>C c.(?_-77)_(*602_?)del	p.Cys35Arg Heterozygous p.0? Heterozygous	Intermediate	F	Vietnamese	Normal	16 yrs, uses wheelchair (ambulant 24–36 mo)	Ventilated 24 hr from 5 yrs. High-arched palate, dysarthria Scoliosis
832-1	c.459delinsACTC	p.Ser153_Ala154insLeu Homozygous	Other forms (grade of severity: mild)	M	Russian	No data	12 yrs, ambulant	Distal weakness > proximal distal contractures
D10-236	c.581_583delAAG c.1238C>T	p.Glu194del Heterozygous p.Ser413Leu Heterozygous	Typical form	M	Chinese	Normal - h 40	5 yrs, ambulant	VSD, finger contractures, focal renal echogenicity
D12-203	c.1748_1755del AAGGAAAT,	p.Lys583Thrfs*7 Homozygous	Fetal akinesia sequence	M	Persian	Polyhydramnios, breech presentation, emergency Cesarean section - h 31+2	Died at 3 mo (active support discontinued)	Arthrogryposis, macrocephaly, hypospadias No antigravity movements at birth
12DG1177	c.641delA	p.Asn214Thrfs*14 Homozygous	Severe form Fetal akinesia sequence	M	Saudi Arabian	Fetal movements weak, breech presentation	Died during 1st day of life	Dislocation of hips and knees, cleft palate, micrognathia, narrow chest

mutations showed a segregation pattern compatible with a recessive mode of inheritance in all families (Figure S1). Severe phenotypes associated with genetic null mutations and intermediate or typical congenital forms with mutations that should results in presence of residual protein, suggests a phenotype-genotype correlation in individuals affected with *KLHL41* mutations.

KLHL41 belongs to the family of BTB-Kelch domain-containing proteins.[17–20] Mutations in two other members of this family, *KBTBD13* (MIM 613727), and most recently *KLHL40* (MIM 615430), have been associated with a clinically distinct form of congenital myopathy exhibiting nemaline bodies, as well as multiminicores and severe NM, respectively.[12,13] To evaluate the impacts of the *KLHL41* mutations on the protein structure, we mapped them onto the crystal structures of the BTB-BACK domain of human KLHL11 in complex with human CUL3, a subunit of E3 ubiquitin ligases, (PDB code 4AP2)[21] and the Kelch domain of rat KLHL41 (PDB code 2WOZ),[22] analogous to those domains of human KLHL41. The Cys35 side chain is involved in a hydrophobic core of the BTB domain, which makes van der Waals contacts with Phe54 of Cul3 (Figure 1B). The p.Cys35Arg substitution present in affected individual 203-1 would likely destabilize the hydrophobic core and thereby impair the interaction with Cul3. This was supported by the FoldX result, in which free energy change upon the p.Cys35Arg substitution was predicted to be over 4 kcal/mol, which can be interpreted as considerable destabilization of a protein structure (Figure 1D; Figure S3).[23] In proband 832-1, a Leu residue is inserted between the amino acid positions 153 and 154 in the center of a helix, in which several residues are involved in a hydrophobic core of the BACK domain (Figure 1B). This amino acid insertion is likely to destabilize the BACK domain fold. In proband D10-236, the p.Ser413Leu substitution was mapped to a loop region, which is located near the substrate-binding region of the Kelch repeat 2 (Figure 1C; Figure S1B). A FoldX calculation predicted that the p.Ser413Leu substitution would have minimal effect on stability of the Kelch domain (Figure 1D). The effect of Glu194 deletion at the N-terminal end of an α helix can be compensated by the presence of Glu193 located in the loop (Figure 1B). Nonetheless, it cannot be excluded that the p.Ser413Leu and p.Glu194del changes alter the protein solubility or aggregate tendency and/or impair substrate binding. The conserved nature of the mutated KLHL41 domains, as well as the potential role of the mutations in disrupting those structural domains, supports the likely pathogenicity of these mutations.

The localization of KLHL41 in skeletal muscles was investigated by immunofluorescence of mouse FDB cultured myofibers and human skeletal muscle cryosections. Immunofluorescence with two different antibodies against N-terminal (Sigma, AV38732) and C-terminal parts of human KLHL41 (Abcam, ab66605) was performed, and z stacks were acquired by confocal microscopy as described

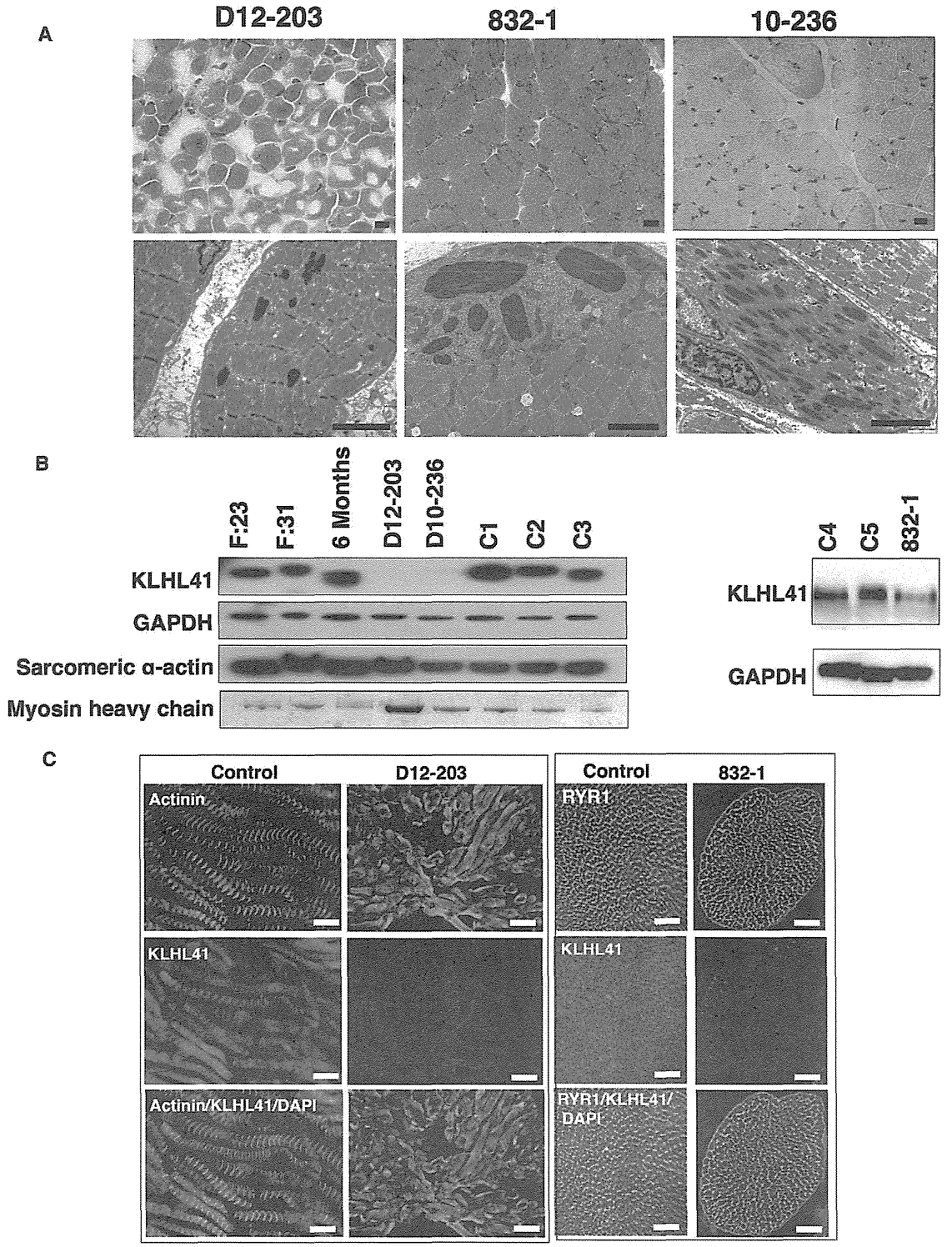

Figure 2. Muscle Pathology and Expression of KLHL41 Levels and Localization in Muscle of Affected Individuals
(A) Light microscopy of Gomori trichrome stained skeletal muscle from affected individuals with *KLHL41* mutations show cytoplasmic nemaline bodies (top panel). Electron microscopy of affected muscles reveals rods of variable frequency and size and severe myofibrillar disarray (bottom panels). (Scale bars represent 2 μm). Affected individuals' IDs are indicated at top.
(B) Immunoblotting analysis of KLHL41 levels in affected and unaffected muscles. A decrease in protein levels was observed in individuals with *KLHL41* mutations in comparison to normal control muscles. Immunoblotting with sarcomeric actin or Coomassie staining of myosin heavy chain showed no abnormal accumulation of sarcomeric proteins in affected muscles. Immunostaining for GAPDH was used for loading controls. Lanes: F:23, 23 week control fetus; F:30, 31 week control fetus; 6-month-old control baby, C1–C5 are normal age-matched control muscles.
(C) Immunofluorescence for KLHL41 in control and affected individual muscle biopsies showed highly reduced levels of KLHL41 in longitudinally oriented (left) or transverse sections (right) of skeletal muscles from affected individuals. Scale bars represent 50 μm.

previously.[24] Immunofluorescence with both antibodies resulted in similar staining patterns; however, due to lower background staining, the C-terminal antibody was used for further studies. Costaining with sarcomeric markers in longitudinal planes showed that KLHL41 staining predominated over the I-bands of the sarcomere and at perinuclear regions in human biopsies (Figure 2C) and murine cultured myofibers (Figure S4). Analysis of transverse sections of myofibers from control human biopsies revealed KLHL41 staining in a ring pattern around the myofibrils, generally colocalizing with ryanodine receptors (RYR1), which are a marker of the sarcoplasmic reticulum (Figure S5). Together, these observations suggest that KLHL41 localizes over (but not within) I bands, likely in association with the terminal cisternae of the sarcomplasmic reticulum (SR) and longitudinal vesicles of the SR present in the I-band area at the triadic regions (Figure S4). Colocalization studies with the ER marker protein disulfide isomerase (PDI) in myofibers and skeletal muscles further confirmed the localization of KLHL41 in SR-ER membranes (Figures S4). This overall localization pattern is most consistent with localization to the endoplasmic reticulum (ER) around myonuclei and to microdomains of the SR with ER characteristics.[25] Previous studies suggested that the closely related NM protein, KLHL40, localized at A-bands,[13] but double label immunofluorescence studies of both longitudinal and transverse sections here reveal that it appears colocalized with RYR1, around but not within the myofibrils in cultured myofibers and human skeletal muscles in a pattern overlapping, but not identical to, that of KLHL41 (Figures S4 and S5). These associations of proteins whose defects cause NM with the ER/SR contrasts with previously known NM proteins, all of which are sarcomeric thin filament components, with the exception of KBTBD13 whose localization is not well known.

In mouse tissues, immunoblotting detected KLHL41 in skeletal muscle and diaphragm (Figure S6). In cultured murine C2C12 cells, KLHL41 levels increased during differentiation to myotubes (Figure S6). Immunoblotting of affected skeletal muscle extracts revealed greatly reduced levels of KLHL41 in individuals with *KLHL41* mutations (Figure 2B) and immunofluorescence microscopy of affected individuals' skeletal muscles also showed that KLHL41 levels were greatly reduced in their myofibers (Figure 2C).

Cell culture studies have shown that KLHL41 interacts with nebulin, N-RAP (Nebulin-related anchoring protein), and actin in skeletal muscle and promotes the assembly of myofibrils.[26] KLHL41 regulates skeletal muscle differentiation as overexpression or knockdown inhibited C2C12 myoblast differentiation.[27] Knockdown of *Klhl41* in cultured cardiomyocytes resulted in sarcomeric disorganization with thickening of Z-lines as seen in NM.[28] However, the exact functions of KLHL41 in disease pathology are unknown. Recent studies have identified mutations in two other closely related family members *KBTBD13* and *KLHL40* as causes of NM suggesting the crucial requirement for several Kelch family proteins in skeletal muscle function.[12,13] To investigate the functional role of KLHL41 in vertebrate skeletal muscle development, we employed zebrafish as a model system. Zebrafish have two duplicated orthologs (*klhl41a* and *klhl41b*) that share ~80% similarity with *KLHL41*. Zebrafish whole-mount in situ hybridization was performed to study the spatio-temporal expression of these genes during zebrafish development as described previously.[29] Specifically, RNA probes specific for each Klhl41 gene were generated by amplification of the 3′ UTRs from a cDNA library of 2 day postfertilization (dpf) zebrafish embryos, followed by in vitro transcription to generate digoxigenin-labeled antisense transcripts (primer sequences are provided in Table S1). Whole-mount in situ hybridization showed ubiquitous expression of *klhl41a* during early development at 1 dpf, but by 2 dpf, *klhl41a* transcripts were virtually undetectable in the major axial skeletal muscles. In contract, *klhl41b* expression was predominantly seen in striated muscles, and strong expression in heart and skeletal muscles was observed throughout zebrafish development to at least 5 dpf (Figure 3A).

The effect of KLHL41 deficiency in zebrafish was studied by knocking down the Klhl41 genes with antisense morpholinos. Two independent morpholinos targeting an exon-intron spice site and translational start site were designed for both genes (morpholino sequences are provided in Table S2). As initial experiments with both morpholinos for each transcript resulted in similar phenotypes, we performed the remainder of our studies with the splice-site morpholinos (7 ng). *klhl41a* morphants exhibited leaner bodies, smaller eyes, and pericardial edema as seen in other myopathy models (n = 65–110) (Figure 3B).[30,31] Examination of 3 dpf morphants with polarized light showed reduced birefringence in axial skeletal muscles suggesting disorganized skeletal muscle structure (Figure 3B; Figure S7). Knockdown of *klhl41b* resulted in reduced birefringence without any other significant abnormalities (n = 82–132). Targeting both *klhl41a* and *klhl41b* (7 ng each) resulted in curved bodies with a 30% reduction in size along with small eyes and pericardial edema (n = 89–103), compared to fish injected with control morpholino (14ng). *klhl41a* morphant fish die by 3 dpf while *klhl41b* morphants typically did not survive past 5 dpf. Knockdown of both genes was lethal by 3 dpf. Double knockdown fish exhibited severely disorganized muscle (measured by reduced birefringence) compared to controls and either of the single knockdowns. RT-PCR and immunoblotting confirmed the knockdown of *klhl41a* and *klhl41b* transcripts and a reduction in protein levels (Figures 3C and 3D). Overexpression of human *KLHL41* mRNA in the double morphants resulted in a significant increase in the number of surviving fish with normal birefringence suggesting the specificity of morpholino injections and demonstrating the ability of this single evolutionary ortholog to complement both zebrafish genes (Figure 3E). Behavioral characterization of 3

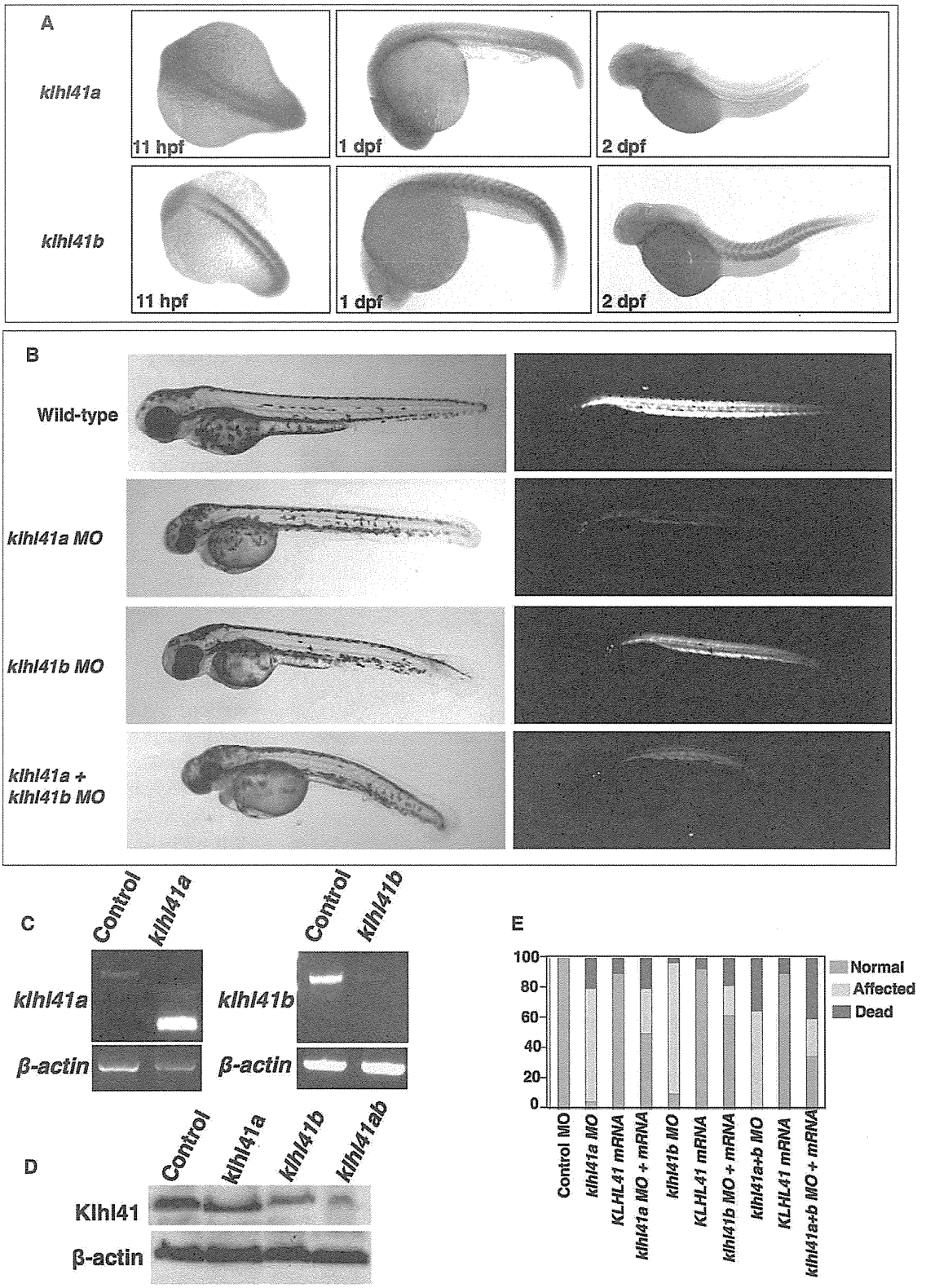

Figure 3. Characterization and Knockdown of Zebrafish Orthologs of *KLHL41*

(A) In situ hybridization of the zebrafish Klhl41 genes shows early expression during myogenesis in developing somites (11 hr after fertilization). *Klhl41a* is expressed in brain, eyes, and muscle at 1 dpf. Later in development expression is largely restricted to brain and heart (2 dpf), although low levels of expression in axial slow skeletal myofibers cannot be excluded due to limited sensitivity of the assay. *Klhl41b* expression is localized to skeletal muscle and heart at all developmental stages (1–2 dpf).

(B) Knockdown of Klhl41 genes in zebrafish using antisense morpholinos results in myopathic changes. Live microscopy of zebrafish embryos at 3 dpf reveals leaner and smaller bodies in comparison to wild-type (WT) fish. Under polarized microscopy, zebrafish embryos

(legend continued on next page)

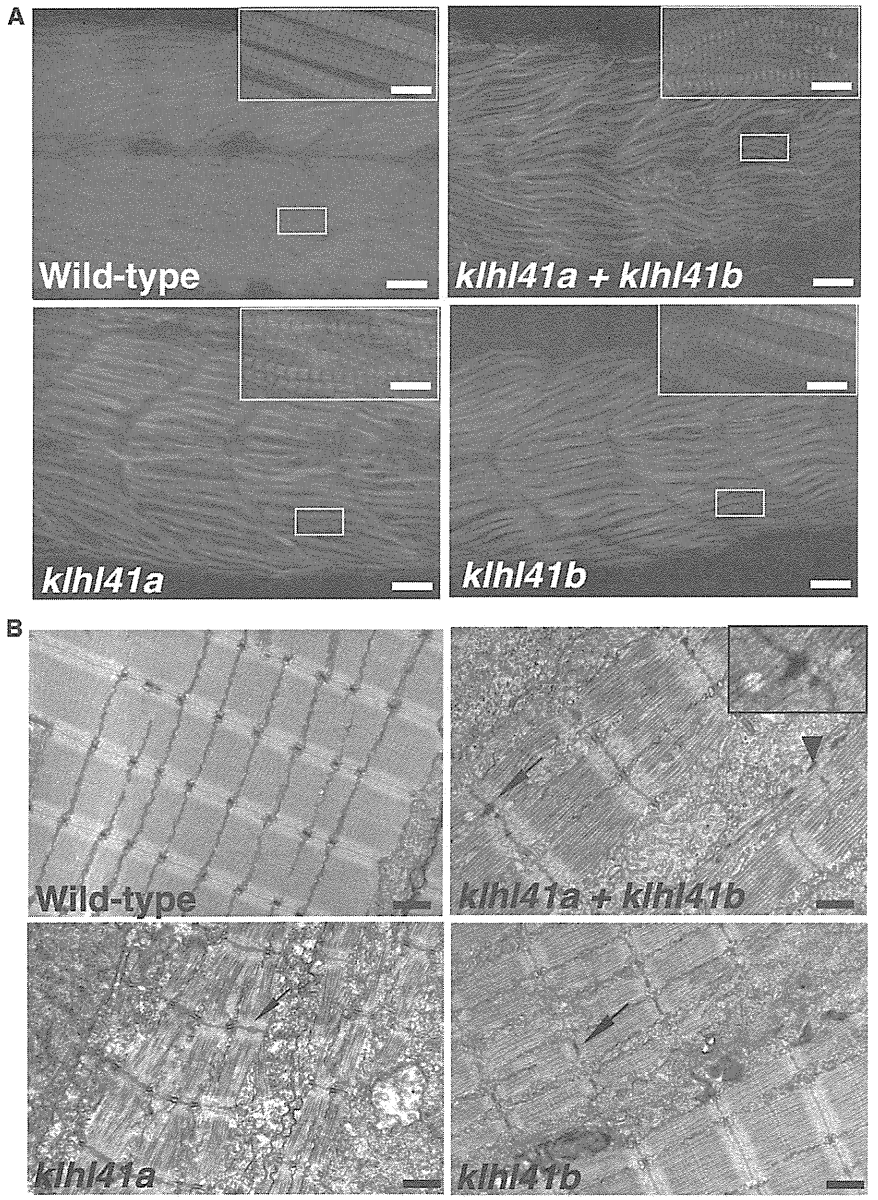

Figure 4. Loss of *klhl41* Function in Zebrafish Recapitulates the Disease Pathology of Human Nemaline Myopathies

(A) Whole-mount staining of 3 dpf zebrafish embryos with phalloidin showed extensive myofibrillar disarray of myofibers in *klhl41* morphant fish (scale bar represents 2 μm). Three dpf embryos fixed in 4% paraformaldehyde were incubated with phalloidin (Invitrogen, A12380, 1:40) overnight at 4°C. Skeletal muscles of klhl41-deficient embryos were smaller and exhibited an overall reduction of myofibrillar organization (inset, high magnification).

(B) Electron microscopy of klhl41-deficient skeletal muscle revealed thickened Z-lines in *klhl41a* or *klhl41b* morphants. In addition, skeletal muscle of double knockdown fish contained electron dense bodies, reminiscent of nascent nemaline rods (arrowhead, nemaline bodies like structures; arrow, thickened Z-lines) (scale bar represents 1 μm).

dpf morphant fish, knocked down for either or both Klhl41 genes, using the touch-evoked response assay showed significantly diminished motility in comparison to control fish (WT fish: 5.74 ± 0.98 cm/0.1 s; *klhl41a*: 1.32 ± 0.61 cm/0.1 s; *klhl41b*: 2.00 ± 0.49 cm/0.1 s; *klhl41ab*: 0.73 ± 0.39 cm/0.1 s), suggesting a significant degree of overall muscle weakness (Movies S1, S2, S3, and S4).[32] To visualize abnormalities in sarcomeric architecture, whole-mount staining of morphant fish and control zebrafish embryos was performed with phalloidin to stain the actin-thin filaments. Although well-organized myofibrillar striations (i.e., sarcomeres) were observed, the myofibrils in *klhl41* morphants tended to be thinner and were highly disorganized relative to control fish (Figure 4A). The myofibrilar disorganization in *klhl41* morphants was also evident by evaluation of ultrathin toluidine blue sections of control and morphant fish (Figure S7). The main diagnostic feature of NM is the presence of nemaline rods with or without Z-line streaming in skeletal muscle. Ultrastructural examination of zebrafish skeletal muscle by electron microscopy showed Z-line thickening in both *klhl41a* and *klhl41b* morphant fish (Figure 4B). Knockdown of both *klhla* and *klhl41b* resulted in the presence of numerous electron-dense structures, reminiscent of small or nascent nemaline bodies, in addition to Z-line thickening (Figure 4B). Given the differences in temporal expression of *klhl41a* (early embryogenesis) and *klhl41b*

exhibit a reduction in birefringence in morphant fish, quantified in ImageJ as described (WT controls: 100% ± 5.9% *klhl41a*: 23% ± 3.0%; *klhl41b*: 31% ± 8.2%; *klhl41ab*: 16% ± 4.2%). Double knockdown fish show a more severe skeletal muscle phenotype than single morphants.

(C) RT-PCR analysis showed knockdown of normal transcripts in the morphant fish.

(D) Immunoblot analysis showed reduction in Klhl41 levels in *klhl41a*, *klhl41b*, and *klhl41ab* fish. Klhl41 antibody recognizes both klhl41a and klhl41b and therefore show immunoreactibility to the other gene in the single morphants that is highly reduced in double morphants.

(E) Overexpression of human *KLHL41* mRNA restores the skeletal muscle phenotypes of *klhl41a/b* single and double morphants suggesting morpholino specificity. The mRNA concentration used to rescue were as follows: *klhl41a* (50 pg), *klhl41b* (75 pg), *klhl41a+b* (60 pg of each).

(maintained later in development), and the high degree of structural and functional conservation (both are rescued by the single human transcript), it is likely that increased severity of *klhl41a* morphants is due to this being the predominant embryonic isoform at the early stages targeted by morpholino injections.

Extensive skeletal muscle disorganization associated with sarcomeric abnormalities in morphant fish points toward a function of KLHL41 in skeletal muscle development and maintenance. Mutations affecting the closely related BTB-Kelch family member KLHL40 have recently also been reported to cause nemaline myopathy.[13] While *KLHL40* mutations resulted in a severe clinical presentation in most of the affected individuals, KLHL41 abnormalities are associated with a spectrum of phenotypes from severe with neonatal death, to survival into late childhood. However, no significant differences were seen in skeletal muscle pathology. KLHL40 contains a putative nuclear localization sequence (NLS) and is expressed throughout muscle differentiation, whereas KLHL41 lacks NLS and is expressed in late differentiation (Figure S8).[13] KLHL41 and many other BTB domain-containing Kelch family members are known to interact with Cul3 ubiquitin ligase to form functional ubiquitination complexes with proteins targeted for degradation.[21,33] KLHL41, which has been shown to interact with nebulin,[34] is now the third BTB-Kelch family member to be identified as a cause of NM when mutated. We hypothesize that improper surveillance and degradation of aberrant thin-filament proteins might explain the convergent pathological and clinical phenotypes associated with mutations of thin filament and BTB-Kelch family member genes in NM.

Supplemental Data

Supplemental Data include eight figures, two tables, and four movies and can be found with this article online at http://www.cell.com/AJHG/home.

Acknowledgments

We are grateful to the many NM affected individuals and their families, and to their treating physicians, for their participation in this research. Whole-exome sequencing was made possible through the generous support and assistance of David Margulies and the entire staff of The Gene Partnership Project at Boston Children's Hospital. We would like to thank Pankaj Agrawal and Wen-Hann Tan for many helpful discussions during the course of this work. We are thankful to Louise Trakimas of the electron microscope facility at Harvard Medical School for excellent help with zebrafish histology, and the Genotyping and Sequencing Core Facilities at KFSHRC for their technical help. V.A.G. is supported by K01 AR062601 from the National Institute of Arthritis and Musculoskeletal and Skin Diseases of National Institute of Health. This work was also supported by the Muscular Dystrophy Association of USA (MDA201302), National Institutes of Health grant from the National Institute of Arthritis and Musculoskeletal and Skin Diseases R01 AR044345, the AUism Charitable Foundation, and A Foundation Building Strength (to A.H.B.); National Health and Medical Research Council of Australia Early Career Researcher Fellowship #1035955 (to G.R.); Research Fellowship APP1002147 and Project Grant APP1022707(to N.G.L.); the Association Française contre les Myopathies (#15734), Dubai-Harvard Foundation for Medical Research Collaborative Research Grant (to F.S.A.); a UWA Collaborative Research Award (G.R.); and the Great Ormond Street Hospital Children's Charity (to F.M.). E.J.T. and K.S.Y. are supported by University of Western Australia Postgraduate Awards. DNA sequencing was performed by the Boston Children's Hospital Genomics Program Molecular Genetics Core, and confocal microscopy was performed at Boston Children's Hospital Intellectual and Developmental Disability Research Center Imaging Core, both supported by National Institutes of Health grant P30 HD18655. The funders had no role in study design, data collection and analysis, decision to publish, or preparation of the manuscript.

Received: August 9, 2013
Revised: October 15, 2013
Accepted: October 22, 2013
Published: November 21, 2013

Web Resources

The URLs for data presented herein are as follows:

1000 Genomes, http://browser.1000genomes.org
dbSNP, http://www.ncbi.nlm.nih.gov/projects/SNP/
NHLBI Exome Sequencing Project (ESP) Exome Variant Server, http://evs.gs.washington.edu/EVS/
Online Mendelian Inheritance in Man (OMIM), http://www.omim.org/
Picard, http://picard.sourceforge.net/
Pymol, http://www.pymol.org

References

1. Wallgren-Pettersson, C., Sewry, C.A., Nowak, K.J., and Laing, N.G. (2011). Nemaline myopathies. Semin. Pediatr. Neurol. *18*, 230–238.
2. Ryan, M.M., Schnell, C., Strickland, C.D., Shield, L.K., Morgan, G., Iannaccone, S.T., Laing, N.G., Beggs, A.H., and North, K.N. (2001). Nemaline myopathy: a clinical study of 143 cases. Ann. Neurol. *50*, 312–320.
3. Wallgren-Pettersson, C. (2002). Nemaline and myotubular myopathies. Semin. Pediatr. Neurol. *9*, 132–144.
4. Sewry, C.A. (2008). Pathological defects in congenital myopathies. J. Muscle Res. Cell Motil. *29*, 231–238.
5. Hutchinson, D.O., Charlton, A., Laing, N.G., Ilkovski, B., and North, K.N. (2006). Autosomal dominant nemaline myopathy with intranuclear rods due to mutation of the skeletal muscle ACTA1 gene: clinical and pathological variability within a kindred. Neuromuscul. Disord. *16*, 113–121.
6. Pelin, K., Hilpelä, P., Donner, K., Sewry, C., Akkari, P.A., Wilton, S.D., Wattanasirichaigoon, D., Bang, M.L., Centner, T., Hanefeld, F., et al. (1999). Mutations in the nebulin gene associated with autosomal recessive nemaline myopathy. Proc. Natl. Acad. Sci. USA *96*, 2305–2310.
7. Nowak, K.J., Wattanasirichaigoon, D., Goebel, H.H., Wilce, M., Pelin, K., Donner, K., Jacob, R.L., Hübner, C., Oexle, K., Anderson, J.R., et al. (1999). Mutations in the skeletal muscle

alpha-actin gene in patients with actin myopathy and nemaline myopathy. Nat. Genet. *23*, 208–212.
8. Laing, N.G., Wilton, S.D., Akkari, P.A., Dorosz, S., Boundy, K., Kneebone, C., Blumbergs, P., White, S., Watkins, H., Love, D.R., et al. (1995). A mutation in the alpha tropomyosin gene TPM3 associated with autosomal dominant nemaline myopathy. Nat. Genet. *9*, 75–79.
9. Tajsharghi, H., Ohlsson, M., Lindberg, C., and Oldfors, A. (2007). Congenital myopathy with nemaline rods and cap structures caused by a mutation in the beta-tropomyosin gene (TPM2). Arch. Neurol. *64*, 1334–1338.
10. Agrawal, P.B., Greenleaf, R.S., Tomczak, K.K., Lehtokari, V.L., Wallgren-Pettersson, C., Wallefeld, W., Laing, N.G., Darras, B.T., Maciver, S.K., Dormitzer, P.R., and Beggs, A.H. (2007). Nemaline myopathy with minicores caused by mutation of the CFL2 gene encoding the skeletal muscle actin-binding protein, cofilin-2. Am. J. Hum. Genet. *80*, 162–167.
11. Johnston, J.J., Kelley, R.I., Crawford, T.O., Morton, D.H., Agarwala, R., Koch, T., Schäffer, A.A., Francomano, C.A., and Biesecker, L.G. (2000). A novel nemaline myopathy in the Amish caused by a mutation in troponin T1. Am. J. Hum. Genet. *67*, 814–821.
12. Sambuughin, N., Yau, K.S., Olivé, M., Duff, R.M., Bayarsaikhan, M., Lu, S., Gonzalez-Mera, L., Sivadorai, P., Nowak, K.J., Ravenscroft, G., et al. (2010). Dominant mutations in KBTBD13, a member of the BTB/Kelch family, cause nemaline myopathy with cores. Am. J. Hum. Genet. *87*, 842–847.
13. Ravenscroft, G., Miyatake, S., Lehtokari, V.L., Todd, E.J., Vornanen, P., Yau, K.S., Hayashi, Y.K., Miyake, N., Tsurusaki, Y., Doi, H., et al. (2013). Mutations in KLHL40 are a frequent cause of severe autosomal-recessive nemaline myopathy. Am. J. Hum. Genet. *93*, 6–18.
14. Li, H., and Durbin, R. (2009). Fast and accurate short read alignment with Burrows-Wheeler transform. Bioinformatics *25*, 1754–1760.
15. Wang, K., Li, M., and Hakonarson, H. (2010). ANNOVAR: functional annotation of genetic variants from high-throughput sequencing data. Nucleic Acids Res. *38*, e164.
16. Alkuraya, F.S. (2012). Discovery of rare homozygous mutations from studies of consanguineous pedigrees. Curr Protoc Hum Genet. *Chapter 6*, Unit 6, 12.
17. Adams, J., Kelso, R., and Cooley, L. (2000). The kelch repeat superfamily of proteins: propellers of cell function. Trends Cell Biol. *10*, 17–24.
18. Dhanoa, B.S., Cogliati, T., Satish, A.G., Bruford, E.A., and Friedman, J.S. (2013). Update on the Kelch-like (KLHL) gene family. Hum. Genomics *7*, 13.
19. du Puy, L., Beqqali, A., van Tol, H.T., Monshouwer-Kloots, J., Passier, R., Haagsman, H.P., and Roelen, B.A. (2012). Sarcosin (Krp1) in skeletal muscle differentiation: gene expression profiling and knockdown experiments. Int. J. Dev. Biol. *56*, 301–309.
20. Gray, C.H., McGarry, L.C., Spence, H.J., Riboldi-Tunnicliffe, A., and Ozanne, B.W. (2009). Novel beta-propeller of the BTB-Kelch protein Krp1 provides a binding site for Lasp-1 that is necessary for pseudopodial extension. J. Biol. Chem. *284*, 30498–30507.
21. Canning, P., Cooper, C.D., Krojer, T., Murray, J.W., Pike, A.C., Chaikuad, A., Keates, T., Thangaratnarajah, C., Hojzan, V., Marsden, B.D., et al. (2013). Structural basis for Cul3 protein assembly with the BTB-Kelch family of E3 ubiquitin ligases. J. Biol. Chem. *288*, 7803–7814.
22. Spence, H.J., Johnston, I., Ewart, K., Buchanan, S.J., Fitzgerald, U., and Ozanne, B.W. (2000). Krp1, a novel kelch related protein that is involved in pseudopod elongation in transformed cells. Oncogene *19*, 1266–1276.
23. Guerois, R., Nielsen, J.E., and Serrano, L. (2002). Predicting changes in the stability of proteins and protein complexes: a study of more than 1000 mutations. J. Mol. Biol. *320*, 369–387.
24. Lawlor, M.W., Alexander, M.S., Viola, M.G., Meng, H., Joubert, R., Gupta, V., Motohashi, N., Manfready, R.A., Hsu, C.P., Huang, P., et al. (2012). Myotubularin-deficient myoblasts display increased apoptosis, delayed proliferation, and poor cell engraftment. Am. J. Pathol. *181*, 961–968.
25. Kaisto, T., and Metsikkö, K. (2003). Distribution of the endoplasmic reticulum and its relationship with the sarcoplasmic reticulum in skeletal myofibers. Exp. Cell Res. *289*, 47–57.
26. Lu, S., Carroll, S.L., Herrera, A.H., Ozanne, B., and Horowits, R. (2003). New N-RAP-binding partners alpha-actinin, filamin and Krp1 detected by yeast two-hybrid screening: implications for myofibril assembly. J. Cell Sci. *116*, 2169–2178.
27. Paxton, C.W., Cosgrove, R.A., Drozd, A.C., Wiggins, E.L., Woodhouse, S., Watson, R.A., Spence, H.J., Ozanne, B.W., and Pell, J.M. (2011). BTB-Kelch protein Krp1 regulates proliferation and differentiation of myoblasts. Am. J. Physiol. Cell Physiol. *300*, C1345–C1355.
28. Greenberg, C.C., Connelly, P.S., Daniels, M.P., and Horowits, R. (2008). Krp1 (Sarcosin) promotes lateral fusion of myofibril assembly intermediates in cultured mouse cardiomyocytes. Exp. Cell Res. *314*, 1177–1191.
29. Gupta, V., Discenza, M., Guyon, J.R., Kunkel, L.M., and Beggs, A.H. (2012). α-Actinin-2 deficiency results in sarcomeric defects in zebrafish that cannot be rescued by α-actinin-3 revealing functional differences between sarcomeric isoforms. FASEB J. *26*, 1892–1908.
30. Dowling, J.J., Vreede, A.P., Low, S.E., Gibbs, E.M., Kuwada, J.Y., Bonnemann, C.G., and Feldman, E.L. (2009). Loss of myotubularin function results in T-tubule disorganization in zebrafish and human myotubular myopathy. PLoS Genet. *5*, e1000372.
31. Gupta, V.A., Kawahara, G., Myers, J.A., Chen, A.T., Hall, T.E., Manzini, M.C., Currie, P.D., Zhou, Y., Zon, L.I., Kunkel, L.M., and Beggs, A.H. (2012). A splice site mutation in laminin-α2 results in a severe muscular dystrophy and growth abnormalities in zebrafish. PLoS ONE *7*, e43794.
32. Smith, L.S., Beggs, A.H., and Gupta, V.A. (2013). Analysis of skeletal muscle defects in larval zebrafish by birefringence and touch-evoke escape response assays. J. Vis. Exp. *82*, e50925. http://dx.doi.org/10.3791/50925.
33. Zhang, D.D., Lo, S.C., Sun, Z., Habib, G.M., Lieberman, M.W., and Hannink, M. (2005). Ubiquitination of Keap1, a BTB-Kelch substrate adaptor protein for Cul3, targets Keap1 for degradation by a proteasome-independent pathway. J. Biol. Chem. *280*, 30091–30099.
34. Spence, H.J., McGarry, L., Chew, C.S., Carragher, N.O., Scott-Carragher, L.A., Yuan, Z., Croft, D.R., Olson, M.F., Frame, M., and Ozanne, B.W. (2006). AP-1 differentially expressed proteins Krp1 and fibronectin cooperatively enhance Rho-ROCK-independent mesenchymal invasion by altering the function, localization, and activity of nondifferentially expressed proteins. Mol. Cell. Biol. *26*, 1480–1495.

Whole genome sequencing in patients with retinitis pigmentosa reveals pathogenic DNA structural changes and *NEK2* as a new disease gene

Koji M. Nishiguchi[a,b], Richard G. Tearle[c], Yangfan P. Liu[d], Edwin C. Oh[d,e], Noriko Miyake[f], Paola Benaglio[a], Shyana Harper[g], Hanna Koskiniemi-Kuendig[a], Giulia Venturini[a], Dror Sharon[h], Robert K. Koenekoop[i], Makoto Nakamura[b], Mineo Kondo[b], Shinji Ueno[b], Tetsuhiro R. Yasuma[b], Jacques S. Beckmann[a,j,k], Shiro Ikegawa[l], Naomichi Matsumoto[f], Hiroko Terasaki[b], Eliot L. Berson[g], Nicholas Katsanis[d], and Carlo Rivolta[a,1]

[a]Department of Medical Genetics, University of Lausanne, 1005 Lausanne, Switzerland; [b]Department of Ophthalmology, Nagoya University School of Medicine, Nagoya 466-8550, Japan; [c]Complete Genomics, Inc., Mountain View, CA 94043; [d]Center for Human Disease Modeling and [e]Department of Neurology, Duke University, Durham, NC 27710; [f]Department of Human Genetics, Yokohama City University Graduate School of Medicine, Yokohama 236-0004, Japan; [g]Berman-Gund Laboratory for the Study of Retinal Degenerations, Harvard Medical School, Massachusetts Eye and Ear Infirmary, Boston, MA 02114; [h]Department of Ophthalmology, Hadassah-Hebrew University Medical Center, Jerusalem 91120, Israel; [i]McGill Ocular Genetics Laboratory, McGill University Health Centre, Montreal, QC, Canada H3H 1P3; [j]Service of Medical Genetics, Lausanne University Hospital, 1011 Lausanne, Switzerland; [k]Swiss Institute of Bioinformatics, 1015 Lausanne, Switzerland; and [l]Laboratory for Bone and Joint Diseases, Center for Genomic Medicine, RIKEN, Tokyo 108-8639, Japan

Edited by Jeremy Nathans, Johns Hopkins University, Baltimore, MD, and approved August 15, 2013 (received for review May 1, 2013)

We performed whole genome sequencing in 16 unrelated patients with autosomal recessive retinitis pigmentosa (ARRP), a disease characterized by progressive retinal degeneration and caused by mutations in over 50 genes, in search of pathogenic DNA variants. Eight patients were from North America, whereas eight were Japanese, a population for which ARRP seems to have different genetic drivers. Using a specific workflow, we assessed both the coding and noncoding regions of the human genome, including the evaluation of highly polymorphic SNPs, structural and copy number variations, as well as 69 control genomes sequenced by the same procedures. We detected homozygous or compound heterozygous mutations in 7 genes associated with ARRP (*USH2A*, *RDH12*, *CNGB1*, *EYS*, *PDE6B*, *DFNB31*, and *CERKL*) in eight patients, three Japanese and five Americans. Fourteen of the 16 mutant alleles identified were previously unknown. Among these, there was a 2.3-kb deletion in *USH2A* and an inverted duplication of ~446 kb in *EYS*, which would have likely escaped conventional screening techniques or exome sequencing. Moreover, in another Japanese patient, we identified a homozygous frameshift (p.L206fs), absent in more than 2,500 chromosomes from ethnically matched controls, in the ciliary gene *NEK2*, encoding a serine/threonine-protein kinase. Inactivation of this gene in zebrafish induced retinal photoreceptor defects that were rescued by human *NEK2* mRNA. In addition to identifying a previously undescribed ARRP gene, our study highlights the importance of rare structural DNA variations in Mendelian diseases and advocates the need for screening approaches that transcend the analysis of the coding sequences of the human genome.

medical genetics | ophthalmology | ciliopathy | retinal blindness

The identification of the genetic causes of rare Mendelian diseases is becoming increasingly important following some success with gene-based therapy, as recently reported for patients with a form of Leber congenital amaurosis (LCA), a severe autosomal recessive hereditary retinal dystrophy (1–3). The evidence that restoring a gene in the diseased retina could yield therapeutic effects has stimulated the pursuit of the genetic causes of other retinal dystrophies, including retinitis pigmentosa (RP).

RP is the name given to a group of hereditary retinal conditions in which degeneration of rod photoreceptors, responsible for vision under starlight or moonlight conditions, is more pronounced than that of cone photoreceptors, which mediate daylight vision. Individuals with RP typically experience night blindness at first, followed by progressive and unstoppable visual impairment in daytime conditions as well (4). Their visual fields become reduced gradually and sight is lost from the midperiphery to the periphery and then from the midperiphery to the center, resulting eventually in complete or near-complete blindness if left untreated. Most patients show intraretinal pigment in a bone spicule configuration around the fundus periphery, for which this condition was named. In addition, they typically show retinal arteriolar attenuation, elevated final dark adapted thresholds, and reduced and delayed electroretinograms (ERGs) (4). Vitamin A supplementation in combination with an omega-3 rich diet can slow the course of retinal degeneration and preserve visual acuity among adults with this condition (5, 6). Autosomal, recessively inherited RP (ARRP) is the most common form of hereditary retinal degeneration in humans. To date, over 50 genes have been associated with ARRP and allied disorders, among patients who are predominantly of European ancestry (RetNet; www.sph.uth.tmc.edu/retnet/home.htm). However, despite this high number of identified disease genes, ~40–50% of all diagnosed cases have no mutations in recognized loci (7). Furthermore, genetic defects in RP are also population specific. For example, a screening of 193 unrelated Japanese patients with isolate or autosomal recessive RP

Significance

Retinitis pigmentosa (RP) is a genetic disease that causes progressive blindness and that is caused by mutations in more than 50 genes. Conventional methods for identification of both RP mutations and novel RP genes involve the screening of DNA sequences spanning coding exons. In our work, we conversely test the use of whole genome sequencing, a technique that takes into account all variants from both the coding and noncoding regions of the human genome. In our approach, we identify a number of unique RP mutations, a previously undescribed disease gene, as well as pathogenic structural DNA rearrangements originating in introns.

Author contributions: K.M.N. and C.R. designed research; K.M.N., Y.P.L., E.C.O., N. Miyake, P.B., H.K.-K., and G.V. performed research; S.H., D.S., R.K.K., M.N., M.K., S.U., T.R.Y., S.I., N. Matsumoto, H.T., and E.L.B. contributed new reagents/analytic tools; K.M.N., R.G.T., Y.P.L., E.C.O., N. Miyake, P.B., H.K.-K., G.V., J.S.B., S.I., N. Matsumoto, N.K., and C.R. analyzed data; and K.M.N., E.C.O., J.S.B., E.L.B., N.K., and C.R. wrote the paper.

Conflict of interest statement: R.G.T. is an employee and shareholder of Complete Genomics, Inc.

This article is a PNAS Direct Submission.

[1]To whom correspondence should be addressed. E-mail: carlo.rivolta@unil.ch.

This article contains supporting information online at www.pnas.org/lookup/suppl/doi:10.1073/pnas.1308243110/-/DCSupplemental.

for 30 disease genes identified commonly within North American or European patients revealed candidate pathogenic mutations in only 14% of the cohort (8).

Recent advances in massively parallel sequencing have enabled the analysis of large amounts of sequences (genes) at reasonable costs, revolutionizing the traditional approach of exon-by-exon Sanger sequencing (9). The two major forms of sequencing strategies allowing large-scale analyses are whole genome sequencing (WGS) and whole exome sequencing (WES). The former reads the entire genome with no distinction between exons and non-exonic regions. It allows the detection of intergenic variants, copy number variations (CNVs), and other structural rearrangements, as well as unrecognized exonic sequences. The latter technique relies on targeted DNA capture and focuses on the analysis of the known exonic content of the genome, performed according to the genomic annotation available at a given point in time.

In this study, we performed WGS as a method for mutation discovery in a highly genetically heterogeneous Mendelian disease; to this end, we evaluated 16 unrelated RP patients from diverse ethnic backgrounds.

Results

Genome Sequencing. Genome sequencing in the 16 analyzed patients produced an average mapping yield of 200.8 ± 17.9 (mean ± SD) Gb and an average coverage of 66.1 ± 2.4 (mean ± SD) reads per base (*SI Appendix*, Table S1). This covered a genomic fraction of 0.968 ± 0.004, in which roughly 3.8 million putative variations were identified. Of these, ~7.7% were not reported in dbSNP build 131 and were classified as novel variants. Variations present within transcripts were classified further as synonymous and nonsynonymous, and analyzed separately for the North American and Japanese sets of patients. Scoring of large structural variations (SVs) could be achieved only for seven genomes, as the remaining DNA samples, possibly because of their older age, did not produce reliable mate pair information (*SI Appendix*, *Results S1*).

Assessment of pathogenic variants was performed by a series of filtering steps, summarized in Fig. 1.

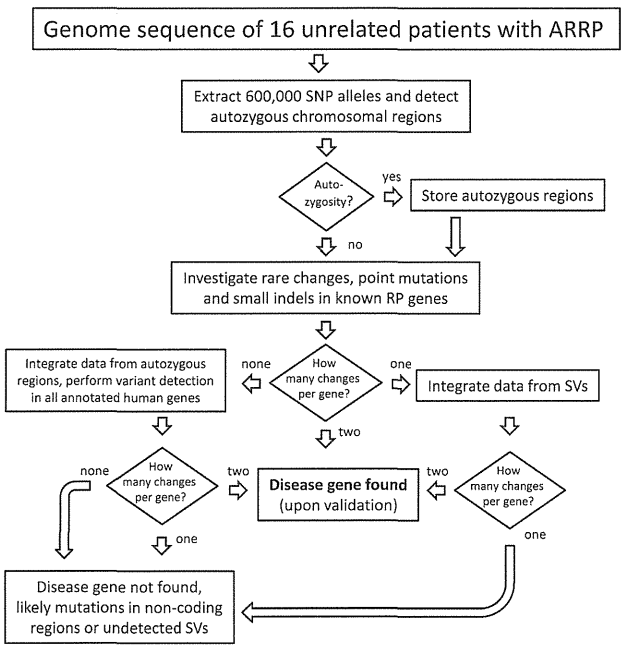

Fig. 1. Flowchart of the filtering process applied in this work.

Assessment of Autozygous Regions. Each genome was evaluated for known or undocumented parental consanguinity as well as for possible founder mutation events by extracting genotypes of known polymorphic SNPs and by searching for long intervals with high degrees of homozygosity (at least 500 consecutive SNP markers, or ~2.2 Mb on average), indicative of identity by descent (IBD). Significant genomic homozygosity was observed only in the five Japanese patients (individual IDs: R14, R15, R16, R18, and R19) who had documented parental consanguinity. The areas of IBD had essentially no overlap among these patients except for a 10-Mb interval on chromosome 1 shared by R15 and R19. Haplotype analysis indicated the shared intervals to be of different origins. No other patients carried genomic areas indicative of IBD; this was consistent with their family history reporting no parental consanguinity.

Sequence Analyses of Known RP Genes. We first focused our analyses on genes known to be associated with ARRP. We investigated both small variants (from 1 to 50 bp) from the mapping of short reads and, whenever possible, large SVs. Our results are summarized in *SI Appendix*, Table S2; detailed results are provided in *SI Appendix*, *Results S1*, Figs. S1 and S3, and Table S3.

In addition to point mutations and short indels (insertion/deletions), we detected pathogenic SVs in *USH2A* and *EYS* in patients 003–019 and R9, respectively, by combining information from sequence coverage and abnormal junctions/mate pair distance. In the genome of patient 003–019, we identified a ~2-kb deletion that removed exon 27 of *USH2A*, whereas patient R9 was found to carry a 446-kb head-to-head inverted duplication of the portion of chromosome 6 that included exons 23–29 of *EYS* (Fig. 2).

We found two pathogenic alleles, in either a homozygous or compound heterozygous state, in 8 of the 16 patients, 5 Americans and 3 Japanese, in seven different genes (*SI Appendix*, Table S2). Six patients carried mutations in one of the following genes: *USH2A*, *RDH12*, *CNGB1*, *EYS*, *PDE6B*, and *DFNB31*; 2 patients had mutations in *CERKL*. None of these mutations were found in the control cohorts of 95 healthy North American or 95 Japanese individuals. None of these mutations were reported previously, except p.R257X in *CERKL* and p.G76R in *RDH12* (10, 11). All mutations cosegregated with RP as recessive, pathogenic alleles in all family members of the index patients for whom DNA samples were available (Fig. 3).

Systematic Screening of All Genes. Based on the data from the analysis of known RP genes, we adopted a pipeline to perform a systematic analysis targeting all annotated genes in the genomes of patients with unsolved genetic etiology (*SI Appendix*, Fig. S2). With the aim of selecting a restricted number of candidate genes, more aggressive filtering was adopted with respect to the one used for the screening of known disease genes. The major differences in the analytical pipeline included removal of all entries in dbSNP. We safely applied this filtering because, given the low frequency of individual mutations in ARRP genes (including undetected ones), the risk of eliminating pathogenic DNA variants that could be fortuitously included in dbSNP build 131 is negligible. Further, to validate this approach, we applied it again retrospectively to the genomes for which mutations in RP genes were already detected. All of identified RP mutations were present in the final list of variants, supporting the sensitivity of the strategy. Detailed results are provided in *SI Appendix*, *Results S2* and are summarized in *SI Appendix*, Figs. S2 and S3 and Table S4.

In R19, in whom we did not find any clear-cut mutations in known ARRP genes, we found a homozygous frameshift variant (p.L206fs, c.617_624delTGTATGAGinsA) in the never in mitosis gene A (NIMA)-related kinase 2 (*NEK2*) gene. This variant was present within a highly homologous genomic stretch of 19.6 Mb of chromosome 1q32, predicted to be IBD (*SI Appendix*, Fig. S4).

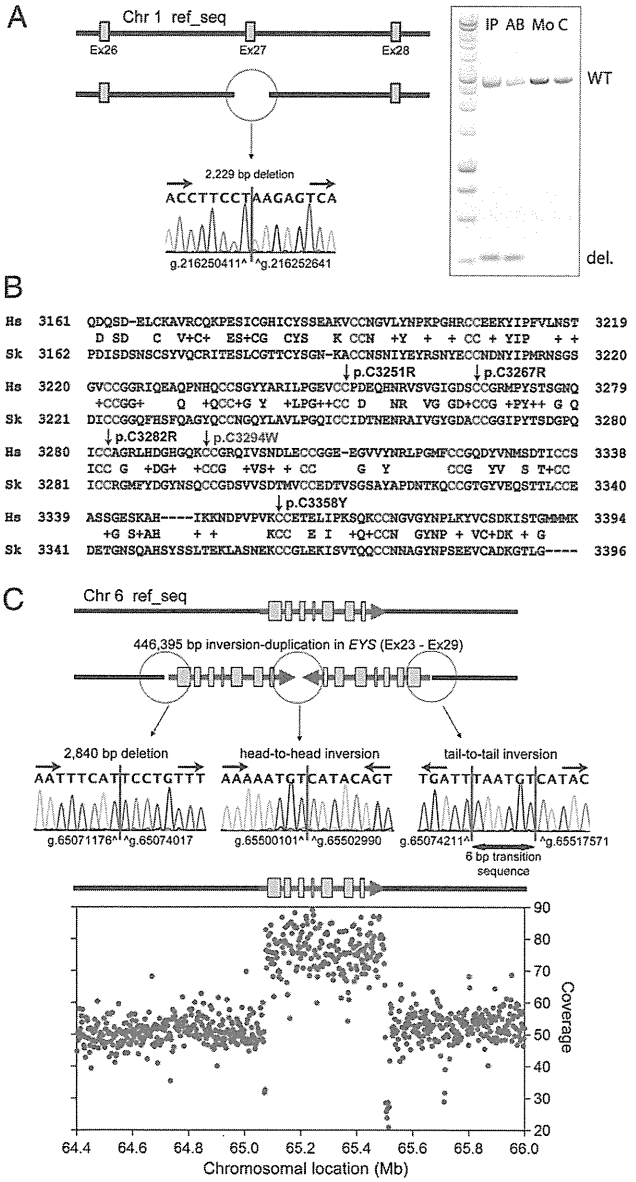

Fig. 2. Pathogenic structural variations identified. (*A*) Sequence of the heterozygous *USH2A* 2,229-bp deletion in patient 003–019 (*Left*) and electrophoresis of the PCR fragments showing a smaller fragment carrying the deletion in the index patient (IP) and her affected brother (AB) but not in her mother (Mo) or a control DNA (C). del, deleted; WT, wild type. (*B*) Alignment of the USH2A protein from *Homo sapiens* (Hs) and *Saccoglossus kowalevskii* (Sk, acorn worm) showing the conservation of 13 CC repeat motifs (red) and the location of the mutation p.C3294W, newly identified in patient 003–019 and her sister. Four previously reported disease-associated missense changes (p.C3251R, p.C3267R, p.C3282R, and p.C3358Y) also affect neighboring CC repeats. (*C*) Schematic representation and DNA sequence of the junctions characterizing the chromosomal rearrangement detected in patient R9 and involving the *EYS* gene. Integration of the information obtained by Sanger DNA sequencing and WGS coverage of the region allows identifying an inverted duplication encompassing exons 23–29.

Similar to most frameshifts producing a premature termination codon, p.L206fs is predicted to result in an mRNA allele that is subject to nonsense-mediated mRNA decay, and therefore in no protein product. Targeted DNA screening revealed that c.617_624delTGTATGAGinsA was absent from 1,273 Japanese and 95 North American control individuals. The entire coding sequence of the *NEK2* gene was then analyzed in a mixed cohort of 190 American patients with ARRP, in 64 Japanese patients with isolate RP, as well as in 13 patients found previously to show linkage between recessive retinal degeneration and the *NEK2* region. However, other than known polymorphisms (rs1056729, rs12031285, and rs45623136), we found only a few isolated heterozygous missense variants (p.R26Q, c.77G>A; p.V137I, c.409G>A; p.I265V, c.793A>G; p.N189S, c.566A>G; and p.K103E, c.307A>G; none were present in dbSNP) insufficient to account for ARRP. Notably, an additional Japanese male with ARRP was found to carry the same frameshift variant p.L206fs, but heterozygously, with no other variants in the *NEK2* coding sequence. This same patient (R51) was later found to carry the retinitis pigmentosa GTPase regulator (*RPGR*) mutation c.2405_2406delAG; p.E802fs (Human Gene Mutation Database entry: CD004115), described previously to be a sufficient cause of RP (12).

In light of a recent study reporting the involvement of noncoding RNA in the pathogenesis of retinal degeneration in mice (13), variants in noncoding RNA were also analyzed. After the removal of variants observed in 52 publicly available control genomes, only isolated heterozygous variants each with one entry per gene remained, insufficient to account for ARRP.

***nek2* Inactivation and Rescue in Zebrafish.** To validate the pathogenic role of *NEK2* deficiency in RP, we suppressed the sole ortholog of *NEK2* in zebrafish embryos and asked whether this manipulation might give rise to photoreceptor phenotypes. Upon injection of 6 ng of *nek2* splice-blocking morpholino, we observed gross ocular defects, including microphthalmia and enlarged eye sockets in 5-d postfertilization (dpf) morphant (MO) embryos (Fig. 4*A*). Whereas 63% of MO embryos displayed such phenotypes, only 21% of embryos expressing both MO and wild-type human *NEK2* mRNA did, suggesting that the ocular phenotypes are specific to the *nek2* suppression ($P < 0.001$) (Fig. 4*B*).

We next asked whether, in addition to overt structural abnormalities that may not directly inform the involvement of this gene to RP in humans, suppression of *nek2* might also give rise to photoreceptor defects consistent with those of patients with ARRP. We therefore embedded and paraffin sectioned control and MO embryos. In addition to the small eye phenotype, we detected alterations in the photoreceptor layer. Specifically, after

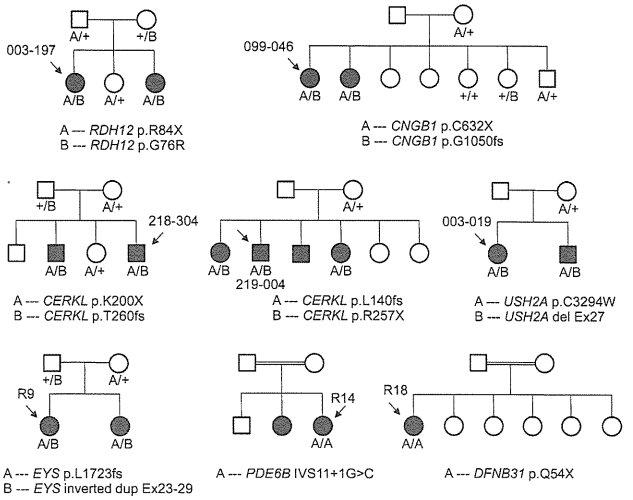

Fig. 3. Cosegregation analyses. All mutations analyzed cosegregated with the disease according to an autosomal recessive pattern of inheritance.

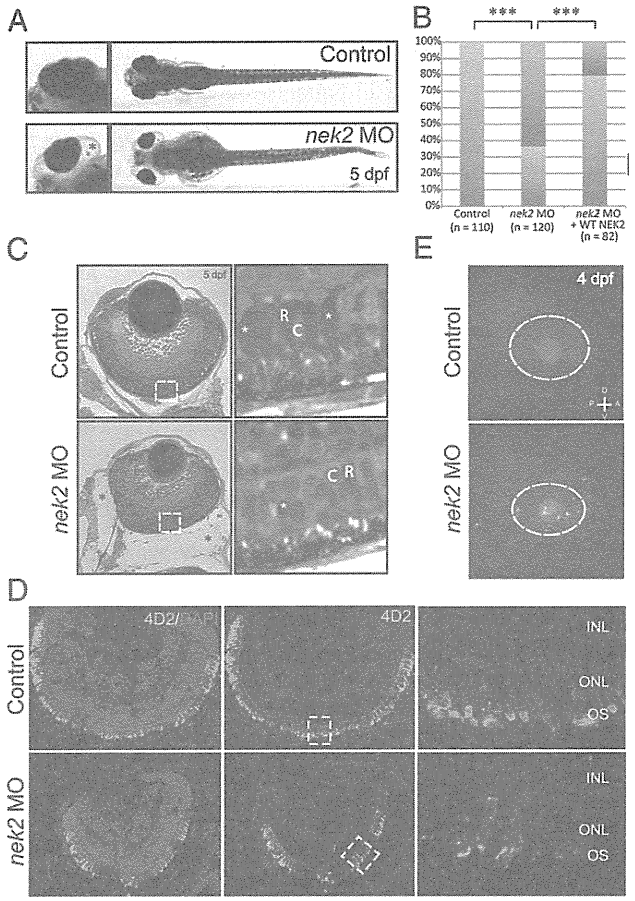

Fig. 4. In vivo functional evaluation of *nek2* loss in zebrafish. (*A*) Bright-field representation of 5-dpf control and *nek2* morphant zebrafish embryos. Magnified *Insets* highlight ocular phenotypes including microphthalmia and enlarged eye sockets (marked by the black asterisk). (*B*) Ocular phenotypes including microphthalmia and enlarged eye sockets vs. normal phenotypes (red bars and blue bars, respectively) are quantified in control and *nek2* morphant embryos, as well as in morphant animals rescued with human WT *NEK2* mRNA. Asterisks indicate statistically significant differences between groups ($P < 0.001$). (*C*) Histology of control and *nek2* morphant embryos also show enlarged eye sockets (marked by black asterisks) and microphthalmia. Magnified *Insets* show a decrease in the number of photoreceptors with apparent changes in domains of condensed chromatin (white asterisks). C, cones; R, rods. (*D*) Immunohistochemical analyses of retinal cryosections from control and *nek2* MO embryos, stained with DAPI (blue) and the 4D2 antibody against rhodopsin (green). Suppression of *nek2* results in the depletion of rods and in the mislocalization of rod opsin from the outer segment (OS) of photoreceptors. INL, inner nuclear layer; ONL, outer nuclear layer. (*E*) TUNEL immunofluorescent images of 4-dpf embryos, showing an increase in the number of apoptotic cells in *nek2* morphant embryos. The dotted ovals indicate the position of the eye. A, anterior; D, dorsal; P, posterior; V, ventral.

serial sectioning of 10–20 embryos injected with sham, MO, or MO + human *NEK2* mRNA, we observed a persistent decrease in the number of photoreceptors with large central domains of condensed chromatin. This phenotype was seen in all *nek2* MO embryos evaluated, but was absent from embryos injected with either sham or MO + human *NEK2* mRNA, suggesting a loss of rod photoreceptors specific to the suppression of *nek2* (Fig. 4*C* and *SI Appendix*, Fig. S5). To verify this observation, we used a rhodopsin (4D2) antibody to stain retinal cryosections from embryos injected with sham, MO, or MO + human *NEK2* mRNA (Fig. 4*D* and *SI Appendix*, Fig. S5). Immunohistochemical analyses of cross-sections from each condition demonstrated that the suppression of *nek2* resulted in the depletion of ~24% of 4D2-positive rod photoreceptors. In addition, mislocalization of rod opsin throughout the photoreceptor cells was evident in the central retina of *nek2* MO specimens, consistent with the hypothesis that nek2 is required for the appropriate trafficking of rhodopsin to the outer segments (Fig. 4*D*).

Further, to ask whether apoptosis, a major mechanism of photoreceptor loss in most known forms of RP (14), might account for some of the observed loss of photoreceptors, we performed TUNEL analysis. Masked scoring of embryos (~50 embryos per injection mixture) revealed a sevenfold increase in the number of TUNEL-positive cells in the eye and head region of *nek2* morphant embryos. By sharp contrast, we did not observe more than 1–10 TUNEL-positive cells in embryos injected with MO + *NEK2* mRNA (Fig. 4*E*).

Finally, we were intrigued by the discovery of a heterozygous frameshift variant p.L206fs in *NEK2* and the bona fide *RPGR* mutation p.E802fs in a patient with RP. We therefore asked whether the *RPGR* variant may interact genetically with the *NEK2* locus. To test this possibility, we coinjected subeffective doses of the *nek2* MO and *rpgr* MO and compared embryos with single or double MO ($n > 100$ at subeffective doses). Approximately 28% of embryos carrying subeffective doses of both *nek2* and *rpgr* MO revealed ocular ($P < 0.001$) and rod photoreceptor phenotypes (serial sectioning of 10 embryos per genotype) that exceeded the number of affected embryos induced by either *nek2* (3%) or *rpgr* (10%) MO alone, suggesting that the RPGR allele interacts *in trans* with the NEK2 locus to exacerbate photoreceptor defects (*SI Appendix*, Fig. S6).

Discussion

Massively parallel sequencing has proven to have a high potential to detect mutations in patients with rare Mendelian diseases (15). To date, most reports focus on monogenic conditions with no genetic heterogeneity, for which mutations can be recognized from benign variants since they invariantly affect the same gene in different patients.

In this study, we explored the efficacy of WGS in identifying mutations in unrelated patients from diverse ethnic backgrounds and presenting with a disease that is clinically the same but that has different genetic drivers. Whereas the small number of genomes analyzed in this study precludes an accurate analysis of quantitative measures, such as sensitivity of the WGS to detect mutations in known RP genes, we observed a few features that allowed us to make some valid comparisons between the different techniques currently available for genetic diagnosis. First, the majority of the pathogenic mutations identified were never reported before. This implies that tools that rely on systematic search for known pathogenic variants, both via mutation-centered resequencing and chip-based hybridization, may not be adequate for ARRP. Second, thanks to full-genome data, we detected complex structural variants whose junctions were located deep in noncoding regions. Because of their nature, these disease-causing variants would have been invisible to standard screening methods, or even to WES. Coverage-based analysis of CNV in exome sequencing has been attempted, with variable results. Limitations of this approach include the uneven efficiency of target DNA capture (and hence sequence coverage, on which assessment of number of copies is based) over different probes and, above all, the low probability of detecting junctions defining the SVs, which are more likely to be found in the nonexonic sequences composing ~98% of our genome. Unambiguous detection of abnormal junctions and mate pair information are crucial parameters in defining a SV; for instance, they allow distinguishing a tandem duplication from an inverted one. Third, because we had access to the full wealth of genomic information, we could integrate many sources of information

at once (e.g., SNP genotypes, phasing, etc.) that allowed us to accurately filter DNA variants that were related to the disease.

Genetic defects in *EYS* were proposed recently to be one of the major causes of ARRP in the Japanese population (16). We found that one of the pathogenic *EYS* alleles was a large SV (446 kb) with a complex genomic rearrangement. This finding supports the notion that SVs represent frequent pathogenic mutations in this gene (17). A homozygous nonsense mutation in exon 6 of *DFNB31* was identified in R18, a patient with nonsyndromic ARRP. The *DFNB31* gene encodes whirlin, a PDZ scaffold protein with expression in both hair cell stereocilia and retinal photoreceptor cells. Whirlin binds to the protein encoded by *USH2A* (18), a gene associated with both Usher syndrome type II (ARRP accompanied by hearing loss) and nonsyndromic ARRP (19). Whereas mutations in *DFNB31* have been reported as rare causes of Usher syndrome type II (20, 21), no DNA changes in its sequence have yet been associated with nonsyndromic ARRP. However, at the age of 66, the past medical history of this patient was significant for only hyperlipidemia and she did not report any hearing loss. We could not perform an auditory examination because she was no longer reachable.

In patients from consanguineous families, regions of IBD allowed restricting the search for pathogenic mutations to only a fraction of the genome. However, these same regions were susceptible to carrying other rare but nonpathogenic homozygous changes as well. Indeed, a higher number of candidate genes/mutations remained among Japanese patients with parental consanguinity compared with those without it (*SI Appendix*, Table S4). These results suggest that even if the analysis should be restricted to areas of IBD, genomes with high homozygosity do not necessarily offer an extra advantage in mutation detection, when comprehensive genomic sequencing in single individuals is performed.

In three patients we identified clear-cut pathogenic but heterozygous mutations in known ARRP genes that could not be associated directly with the disease. This was particularly evident for patient R14, who carried a heterozygous frameshift in *DFNB31* but was also homozygous for a mutation inactivating *PDE6B* (22). These findings are not surprising, given the elevated number of recessive ARRP mutations that are predicted to be present in the general population. Based both on theoretical assessments and on experimental data from control cohorts, we estimated that 1 in 3–7 individuals could be potential heterozygous carriers of an ARRP mutation (23, 24) or, as in the present case, 3 in 16.

The reasons why no candidate mutations of similar quality (i.e., two mutations, at least one of them being clearly deleterious in nature) to those revealed in known RP genes was uncovered in most of the unresolved genomes are unknown. Explanations for this observation may include the presence of variants or SVs that were undetected because of problems inherent in the mapping or sequencing procedure, or of less obvious pathogenic changes that alter splicing or transcription. These would include variants located in introns or in promoter regions, synonymous changes, or changes lying within important yet unannotated exons, genes, or genetic elements that have not been explored in the current study. Diseases caused by oligogenic modes of inheritance, or perhaps attributable to missense mutations for which efficient prioritization is difficult, is another possible explanation. De novo mutations in unknown dominant RP genes could also be evoked.

The search for mutations in unknown disease-causing genes revealed a number of genes with two nonsynonymous changes, which were mostly previously undescribed missenses. Application of more stringent filtering criteria by imposing the presence of at least one deleterious mutation followed by targeted annotation highlighted a single candidate, *NEK2*, in a Japanese patient who carried a homozygous frameshift in this gene. The serine/threonine-protein kinase NEK2 is known to play an important role in regulation of cell cycle progression through localization to the centrosomes and interaction with microtubules (25). The identified frameshift would result either in the creation of premature stop codon yielding a null allele or (less likely) a truncated protein lacking kinase activity and loss of microtubule binding. Importantly, defects in members of the Nek kinase family have been linked to impaired ciliogenesis and polycystic kidney disease (26). Recently, a role for *Nek2* in the left–right patterning of vital organs (a phenotype associated with ciliary function) was established in *Xenopus laevis* (27). In the same work, in situ hybridization revealed the expression of *nek2* transcripts in the eye (27). Furthermore, because NEK2 interacts with and can phosphorylate rootletin, a component of photoreceptor cilia (28, 29), *NEK2* was considered to be an important candidate for ARRP.

Our zebrafish studies showed that lack of Nek2 induces microphthalmia as a gross morphological phenotype. More importantly, in *nek2* morphants, we observed mistrafficking of rhodopsin, a hallmark of photoreceptor disease (30), and a reduced number of rod photoreceptors, likely via apoptotic processes. These phenotypes were rescued by injection of wild-type human *NEK2* mRNA, validating the specificity of the induced defects. Microphthalmia is a phenotype that is difficult to interpret in the present context but that is not uncommon to zebrafish models of RP (31, 32). Meanwhile, photoreceptor death, mistrafficking of rhodospsin, and reduction of the outer retinal layers are classical features of RP in both patients and animal models (7, 14, 33). Indeed, no microphthalmia was noted in patient R19.

Intriguingly, the *NEK2* frameshift identified in R19 was also present in R51, another patient with RP who had a deleterious mutation in *RPGR*. As the *RPGR* mutation in itself could explain the disease, an obvious question was whether the *NEK2* mutation might in fact represent a common benign allele. We therefore searched for this variant in 1,273 control Japanese individuals and found that none carried it (allele frequency $<3.9 \times 10^{-4}$). The p.L206fs mutation in *NEK2* is therefore exceedingly rare, such that its presence in a homozygous state in a patient is a strong argument in favor of its being an uncommon cause for ARRP. Although it is possible to attribute the presence of both *NEK2* and *RPGR* mutations in R51 to chance, a more parsimonious explanation is that mutations in these two genes, both expressed in the connecting cilium, act synergistically to define a severe RP phenotype, due to the established principles of mutational load and oligogenic interactions of pathogenic alleles (34). In turn, this would increase the likelihood for the patient of being examined at earlier ages and analyzed genetically. Multiple genetic modifier genes have been reported for cilia-encoding genes and especially for RPGR (35). These modifiers may account in part for the wide phenotypic spectrum associated with genetic defects in this gene, ranging from localized macular atrophy to retinitis pigmentosa of variable severity. To investigate the possibility of the cooperative effect between deficiencies in these two ciliary genes, we performed in vivo genetic interaction studies and showed that loss of Rpgr function can exacerbate Nek2 ocular phenotypes, including defects comprising the trapping of rhodopsin in the inner segment. Taken together, our genetic and functional data indicate that *NEK2* is a disease gene and that the retinal phenotype that results from its deficiency may represent a newly recognized ciliopathy.

To date, WGS has not been as widely explored as WES in the context of mutation detection. This can be attributed mainly to cost-related issues, because WGS is at least twice as expensive as WES procedures ensuring the same average coverage. We believe that the additional features displayed by WGS are worth the difference in price; however, this is a rather subjective matter that also depends on the disease that is being investigated. In the present case, WGS was essential to identify two pathogenic structural variations originating in introns. This is a significant finding, considering that only seven genomes could undergo SV analysis. Therefore, as a general rule, WGS is probably the strategy of

choice when detection of structural variants or mutations in noncoding regions represents an important element of investigation. In the long term, considering that costs associated with massively parallel sequencing technology is expected to fall further and that analysis pipelines continue to evolve, it is probable that WGS would be just as workable economically and physically as WES. Limitations of WGS include the requirement of high-quality DNA to explore the full leverage of the mate-pair mapping and the lack of reliable pipelines to detect SVs ranging in size from 50 to a few hundred base pairs. Unexpectedly, the difficulty accompanied by handling the large amount of data produced by WGS was not a significant obstacle, given the power of desktop computers presently available on the market. Whereas samples with suitable quality could be obtained through careful preparation of fresh DNA samples, under detection of SVs may be a more problematic issue to solve. This occurs because current mapping is based on two steps: mapping of the short reads aimed at detecting variations between 1 and 50 bp and mate-pair mapping for detection of SVs larger than a few hundred bases; to our knowledge, a solution that could fill the gap between these two mapping approaches remains to be found.

In conclusion, in this study we identified clear-cut causative mutations among the overwhelming number of DNA variants present in the human genome, in single patients from genetically diverse populations. This happened without ambiguities in a highly heterogeneous disease, ARRP, and in more than 50% of the individuals analyzed. Furthermore, two cases presented mutations involving noncoding parts of the genome. Considering that the majority of patients referred for molecular genetics diagnosis are isolated individuals, our results are relevant not only to basic research, but also to future clinical genetic testing.

Methods

Our research protocol involving humans and animals was approved by the institutional review boards of our respective universities and organizations. Written informed consent for providing medical information and blood samples was obtained from each patient. Experimental procedures are described in detail in *SI Appendix, Methods*.

ACKNOWLEDGMENTS. We thank Anna M. Siemiatkowska and Frans P. M. Cremers for sharing material from a person with RP, Adriana Ransijn for technical help, as well as Andrea Superti-Furga, and Luisa Bonafé for fruitful suggestions. Data storage was ensured by the Vital-IT Center for high-performance computing of the Swiss Institute of Bioinformatics. This work was supported by the Swiss National Science Foundation (Grant 310030_138346) and the Gebert Rüf Foundation, Switzerland (Rare Diseases-New Technologies Grant) (both to C.R.); a Center Grant from the Foundation Fighting Blindness (to E.L.B.); National Institutes of Health Grants DK072301 and MH-084018 (to N.K.); Ministry of Health, Labor and Welfare (MHLW) of Japan [Grant 23300101 (to S.I. and N. Matsumoto) and Grant 23300201 (to S.I.)]; MHLW, the Japan Science and Technology Agency, and the Strategic Research Program for Brain Sciences (N. Matsumoto); and a Grant-in-Aid for Scientific Research on Innovative Areas (transcription cycle) from the Ministry of Education, Culture, Sports, Science and Technology of Japan and the Takeda Science Foundation (to N. Matsumoto).

1. Maguire AM, et al. (2008) Safety and efficacy of gene transfer for Leber's congenital amaurosis. *N Engl J Med* 358(21):2240–2248.
2. Bainbridge JW, et al. (2008) Effect of gene therapy on visual function in Leber's congenital amaurosis. *N Engl J Med* 358(21):2231–2239.
3. Cideciyan AV, et al. (2008) Human gene therapy for RPE65 isomerase deficiency activates the retinoid cycle of vision but with slow rod kinetics. *Proc Natl Acad Sci USA* 105(39):15112–15117.
4. Berson EL (1993) Retinitis pigmentosa. The Friedenwald Lecture. *Invest Ophthalmol Vis Sci* 34(5):1659–1676.
5. Berson EL, Rosner B, Sandberg MA, Weigel-DiFranco C, Willett WC (2012) ω-3 intake and visual acuity in patients with retinitis pigmentosa receiving vitamin A. *Arch Ophthalmol* 130(6):707–711.
6. Berson EL, et al. (1993) A randomized trial of vitamin A and vitamin E supplementation for retinitis pigmentosa. *Arch Ophthalmol* 111(6):761–772.
7. Hartong DT, Berson EL, Dryja TP (2006) Retinitis pigmentosa. *Lancet* 368(9549): 1795–1809.
8. Jin ZB, et al. (2008) Identifying pathogenic genetic background of simplex or multiplex retinitis pigmentosa patients: A large scale mutation screening study. *J Med Genet* 45(7):465–472.
9. Tucker T, Marra M, Friedman JM (2009) Massively parallel sequencing: The next big thing in genetic medicine. *Am J Hum Genet* 85(2):142–154.
10. Tuson M, Marfany G, Gonzàlez-Duarte R (2004) Mutation of CERKL, a novel human ceramide kinase gene, causes autosomal recessive retinitis pigmentosa (RP26). *Am J Hum Genet* 74(1):128–138.
11. Aldahmesh MA, et al. (2009) Molecular characterization of retinitis pigmentosa in Saudi Arabia. *Mol Vis* 15:2464–2469.
12. Vervoort R, et al. (2000) Mutational hot spot within a new RPGR exon in X-linked retinitis pigmentosa. *Nat Genet* 25(4):462–466.
13. Sanuki R, et al. (2011) miR-124a is required for hippocampal axogenesis and retinal cone survival through Lhx2 suppression. *Nat Neurosci* 14(9):1125–1134.
14. Cottet S, Schorderet DF (2009) Mechanisms of apoptosis in retinitis pigmentosa. *Curr Mol Med* 9(3):375–383.
15. Rabbani B, Mahdieh N, Hosomichi K, Nakaoka H, Inoue I (2012) Next-generation sequencing: Impact of exome sequencing in characterizing Mendelian disorders. *J Hum Genet* 57(10):621–632.
16. Hosono K, et al. (2012) Two novel mutations in the EYS gene are possible major causes of autosomal recessive retinitis pigmentosa in the Japanese population. *PLoS ONE* 7(2):e31036.
17. Pieras JI, et al. (2011) Copy-number variations in EYS: A significant event in the appearance of arRP. *Invest Ophthalmol Vis Sci* 52(8):5625–5631.
18. van Wijk E, et al. (2006) The DFNB31 gene product whirlin connects to the Usher protein network in the cochlea and retina by direct association with USH2A and VLGR1. *Hum Mol Genet* 15(5):751–765.
19. Rivolta C, Sweklo EA, Berson EL, Dryja TP (2000) Missense mutation in the USH2A gene: Association with recessive retinitis pigmentosa without hearing loss. *Am J Hum Genet* 66(6):1975–1978.
20. Ebermann I, et al. (2007) A novel gene for Usher syndrome type 2: Mutations in the long isoform of whirlin are associated with retinitis pigmentosa and sensorineural hearing loss. *Hum Genet* 121(2):203–211.
21. Yang J, et al. (2010) Ablation of whirlin long isoform disrupts the USH2 protein complex and causes vision and hearing loss. *PLoS Genet* 6(5):e1000955.
22. McLaughlin ME, Sandberg MA, Berson EL, Dryja TP (1993) Recessive mutations in the gene encoding the beta-subunit of rod phosphodiesterase in patients with retinitis pigmentosa. *Nat Genet* 4(2):130–134.
23. Rivolta C, Sharon D, DeAngelis MM, Dryja TP (2002) Retinitis pigmentosa and allied diseases: Numerous diseases, genes, and inheritance patterns. *Hum Mol Genet* 11(10): 1219–1227.
24. Nishiguchi KM, Rivolta C (2012) Genes associated with retinitis pigmentosa and allied diseases are frequently mutated in the general population. *PLoS ONE* 7(7):e41902.
25. Fry AM, Meraldi P, Nigg EA (1998) A centrosomal function for the human Nek2 protein kinase, a member of the NIMA family of cell cycle regulators. *EMBO J* 17(2): 470–481.
26. Quarmby LM, Mahjoub MR (2005) Caught Nek-ing: Cilia and centrioles. *J Cell Sci* 118(Pt 22):5161–5169.
27. Fakhro KA, et al. (2011) Rare copy number variations in congenital heart disease patients identify unique genes in left-right patterning. *Proc Natl Acad Sci USA* 108(7): 2915–2920.
28. Bahe S, Stierhof YD, Wilkinson CJ, Leiss F, Nigg EA (2005) Rootletin forms centriole-associated filaments and functions in centrosome cohesion. *J Cell Biol* 171(1):27–33.
29. Yang J, et al. (2002) Rootletin, a novel coiled-coil protein, is a structural component of the ciliary rootlet. *J Cell Biol* 159(3):431–440.
30. Hollingsworth TJ, Gross AK (2012) Defective trafficking of rhodopsin and its role in retinal degenerations. *Int Rev Cell Mol Biol* 293:1–44.
31. Luo N, Lu J, Sun Y (2012) Evidence of a role of inositol polyphosphate 5-phosphatase INPP5E in cilia formation in zebrafish. *Vision Res* 75:98–107.
32. Patil SB, Hurd TW, Ghosh AK, Murga-Zamalloa CA, Khanna H (2011) Functional analysis of retinitis pigmentosa 2 (RP2) protein reveals variable pathogenic potential of disease-associated missense variants. *PLoS ONE* 6(6):e21379.
33. Chang GQ, Hao Y, Wong F (1993) Apoptosis: Final common pathway of photoreceptor death in rd, rds, and rhodopsin mutant mice. *Neuron* 11(4):595–605.
34. Davis EE, Katsanis N (2012) The ciliopathies: A transitional model into systems biology of human genetic disease. *Curr Opin Genet Dev* 22(3):290–303.
35. Fahim AT, et al. (2011) Allelic heterogeneity and genetic modifier loci contribute to clinical variation in males with X-linked retinitis pigmentosa due to RPGR mutations. *PLoS ONE* 6(8):e23021.

ARTICLE

De Novo Mutations in *GNAO1*, Encoding a $G\alpha_o$ Subunit of Heterotrimeric G Proteins, Cause Epileptic Encephalopathy

Kazuyuki Nakamura,[1,2,9] Hirofumi Kodera,[1,9] Tenpei Akita,[3,9] Masaaki Shiina,[4] Mitsuhiro Kato,[2] Hideki Hoshino,[5] Hiroshi Terashima,[5] Hitoshi Osaka,[6] Shinichi Nakamura,[7] Jun Tohyama,[8] Tatsuro Kumada,[3] Tomonori Furukawa,[3] Satomi Iwata,[3] Takashi Shiihara,[2,10] Masaya Kubota,[5] Satoko Miyatake,[1] Eriko Koshimizu,[1] Kiyomi Nishiyama,[1] Mitsuko Nakashima,[1] Yoshinori Tsurusaki,[1] Noriko Miyake,[1] Kiyoshi Hayasaka,[2] Kazuhiro Ogata,[4] Atsuo Fukuda,[3] Naomichi Matsumoto,[1,*] and Hirotomo Saitsu[1,*]

Heterotrimeric G proteins, composed of α, β, and γ subunits, can transduce a variety of signals from seven-transmembrane-type receptors to intracellular effectors. By whole-exome sequencing and subsequent mutation screening, we identified de novo heterozygous mutations in *GNAO1*, which encodes a $G\alpha_o$ subunit of heterotrimeric G proteins, in four individuals with epileptic encephalopathy. Two of the affected individuals also showed involuntary movements. Somatic mosaicism (approximately 35% to 50% of cells, distributed across multiple cell types, harbored the mutation) was shown in one individual. By mapping the mutation onto three-dimensional models of the Gα subunit in three different complexed states, we found that the three mutants (c.521A>G [p.Asp174Gly], c.836T>A [p.Ile279Asn], and c.572_592del [p.Thr191_Phe197del]) are predicted to destabilize the Gα subunit fold. A fourth mutant (c.607G>A), in which the Gly203 residue located within the highly conserved switch II region is substituted to Arg, is predicted to impair GTP binding and/or activation of downstream effectors, although the p.Gly203Arg substitution might not interfere with Gα binding to G-protein-coupled receptors. Transient-expression experiments suggested that localization to the plasma membrane was variably impaired in the three putatively destabilized mutants. Electrophysiological analysis showed that $G\alpha_o$-mediated inhibition of calcium currents by norepinephrine tended to be lower in three of the four $G\alpha_o$ mutants. These data suggest that aberrant $G\alpha_o$ signaling can cause multiple neurodevelopmental phenotypes, including epileptic encephalopathy and involuntary movements.

Introduction

Epileptic encephalopathy is a group of neurological disorders characterized by severe and progressive cognitive and behavioral impairments, which are most likely caused or made worse by epileptic activity.[1] Ohtahara syndrome (OS [MIM 308350 and 612164]) is the most severe and the earliest form of epileptic encephalopathy and is characterized by tonic spasms mainly in the neonatal period, seizure intractability, and a suppression-burst pattern on electroencephalography (EEG).[2] De novo mutations in three genes, *ARX* (MIM 300382), *STXBP1* (MIM 602926), and *KCNQ2* (MIM 602235), have been reported in individuals with OS.[3–6]

Heterotrimeric guanine-binding proteins (G proteins) are composed of α, β, and γ subunits. In its basal state, Gα is bound with guanosine diphosphate (GDP) and forms the Gαβγ complex. When a seven-transmembrane-type receptor binds its agonist, it activates G proteins by catalyzing the exchange of GDP for guanosine triphosphate (GTP) on the Gα subunit. Subsequently, GTP-bound Gα dissociates from Gβγ, and each of the two complexes activates distinct downstream effectors.[7] In mammals, Gα subunits are divided into four classes: $G\alpha_{i/o}$, $G\alpha_{q/11}$, $G\alpha_s$, and $G\alpha_{12/13}$.[7] $G\alpha_o$, encoded by *GNAO1* (MIM 139311), is extremely abundant in brain tissue, where it can constitute up to approximately 0.5% of membrane protein,[8] suggesting important roles in brain function. In fact, mice lacking $G\alpha_o$ show multiple neurological abnormalities, including generalized tremor, occasional seizures, severe motor-control impairment, hyperalgesia, and behavioral abnormalities with early postnatal lethality.[9,10]

In this study, de novo *GNAO1* mutations were identified in four epileptic-encephalopathy-affected individuals, three of whom were diagnosed with OS. In addition, two of the four individuals showed involuntary movements, suggesting that aberration of $G\alpha_o$ can cause multiple neurodevelopmental phenotypes.

[1]Department of Human Genetics, Yokohama City University Graduate School of Medicine, 3-9 Fukuura, Kanazawa-ku, Yokohama 236-0004, Japan; [2]Department of Pediatrics, Yamagata University Faculty of Medicine, 2-2-2 Iida-nishi, Yamagata 990-9585, Japan; [3]Department of Neurophysiology, Hamamatsu University School of Medicine, 1-20-1 Handayama, Higashi-ku, Hamamatsu 431-3192, Japan; [4]Department of Biochemistry, Yokohama City University Graduate School of Medicine, 3-9 Fukuura, Kanazawa-ku, Yokohama 236-0004, Japan; [5]Division of Neurology, National Center for Child Health and Development, 2-10-1 Okura, Setagaya-ku, Tokyo 157-8535, Japan; [6]Division of Neurology, Clinical Research Institute, Kanagawa Children's Medical Center, 2-138-4 Mutsukawa, Minami-ku, Yokohama 232-8555, Japan; [7]Department of Pediatrics, Nagano Red Cross Hospital, 5-22-1 Wakasato, Nagano 380-8582, Japan; [8]Department of Pediatrics, Epilepsy Center, Nishi-Niigata Chuo National Hospital, Niigata 950-2085, Japan
[9]These authors contributed equally to this work
[10]Present address: Department of Neurology, Gunma Children's Medical Center, 779 Shimohakoda Hokkitsu-machi, Shibukawa, Gunma 377-8577, Japan
*Correspondence: naomat@yokohama-cu.ac.jp (N.M.), hsaitsu@yokohama-cu.ac.jp (H.S.)
http://dx.doi.org/10.1016/j.ajhg.2013.07.014.

Subjects and Methods

Subjects

Twelve individuals with OS were previously analyzed by whole-exome sequencing (WES).[3,11] In addition, we analyzed parental samples from 5 of the 12 individuals by WES. Screening for *GNAO1* mutations was performed in 367 individuals with epileptic encephalopathy (including 62 OS cases) by high-resolution-melting (HRM) analysis (339 cases) and/or WES (100 cases). The diagnosis was made on the basis of clinical features and characteristic patterns on EEG. Experimental protocols were approved by the institutional review board of Yokohama City University School of Medicine and Yamagata University Faculty of Medicine. Informed consent was obtained from the families of all individuals.

DNA Samples

Genomic DNA was obtained from peripheral-blood leukocytes by standard methods. For detection of a mosaic mutation in individual 2, genomic DNA from saliva and nails was isolated with an Oragene DNA kit (DNA Genotek) and an ISOHAIR kit (Nippon Gene), respectively.

WES

Genomic DNA was captured with the SureSelect Human All Exon v.4 Kit (Agilent Technologies) and sequenced with four samples per lane on an Illumina HiSeq 2000 (Illumina) with 101 bp paired-end reads. Image analysis and base calling were performed by Sequencing Control Software with Real-Time Analysis and CASAVA software v.1.8 (Illumina). Exome data processing, variant calling, and variant annotation were performed as previously described.[12–14] Reads were aligned to GRCh37 with Novoalign (Novocraft Technologies). Duplicate reads were removed with Picard, and local realignments around indels and base-quality-score recalibration were performed with the Genome Analysis Toolkit (GATK).[13] Single-nucleotide variants and small indels were identified with the GATK UnifiedGenotyper and were filtered according to the Broad Institute's best-practice guidelines v.3. Not flagged as clinically associated, variants registered in dbSNP135 were filtered. Filter-passed variants were annotated with ANNOVAR.[14] Pathogenic mutations detected by WES were confirmed by Sanger sequencing.

Mutation Screening

Genomic DNA was amplified with an illustra GenomiPhi V2 DNA Amplification Kit (GE Healthcare). Exons 1–8 covering the *GNAO1* coding region of two transcript variants (transcript variant 1, RefSeq accession number NM_020988.2, encoding $G\alpha_{o1}$; transcript variant 2, RefSeq accession number NM_138736.2, encoding $G\alpha_{o2}$) were screened by HRM analysis. The last two exons differ between the transcript variants. HRM analysis was performed with a Light Cycler 480 (Roche Diagnostics). Samples showing an aberrant melting curve in the HRM analysis were sequenced. PCR primers and conditions are shown in Table S1, available online. All mutations not present in publically available databases were verified with original genomic DNA and were searched for in the variant database of our 408 in-house control exomes.

Deep Sequencing of a Mosaic Mutation

PCR products (length 178 bp) spanning the c.521A>G mutation were amplified with the use of blood, saliva, and nail DNA samples from individual 2 and blood DNA samples from her parents as a template. Adaptor ligation, nick repair, and amplification were performed with the Ion Xpress Plus Fragment Library Kit (Life Technologies) according to the manufacturer's protocol (part no. 4471989 Rev. B). Indexing was carried out with the Xpress Barcode Adapters 1–16 Kit (Life Technologies). Emulsion PCR and enrichment steps were carried out with the Ion OneTouch 200 Template Kit v.2 (Life Technologies) according to the manufacturer's protocol (part no. 4478371 Rev. A). Sequencing of the amplicon libraries was carried out on the Ion Torrent Personal Genome Machine (PGM) with the Ion 314 sequencing chip and the Ion PGM 200 Sequencing Kit (Life Technologies) according to the recommended protocol (part no. 4474246 Rev. B). Torrent Suite 2.2 was used for all analyses. The percentage of mosaicism was examined with the Integrative Genomics Viewer.[15,16]

Expression Vectors

A full-length human *GNAO1* cDNA clone (transcript variant 1, encoding $G\alpha_{o1}$) was purchased from Kazusa DNA Research Institute. Human *GNAO1* cDNA was inserted into a pEF6/V5-His-C vector for the introduction of a C-terminal V5 epitope (Life Technologies). Site-directed mutagenesis using a KOD-Plus-Mutagenesis kit (Toyobo) was performed for generating *GNAO1* mutants, including c.521A>G (p.Asp174Gly), c.572_592del (p.The191_Phe197del), c.836T>A (p.Ile279Asn), and c.607G>A (p.Gly203Arg). A c.607_609delinsACA (p.Gly203Thr) mutant, in which GTP binding was reversible in contrast to the WT,[17] was also generated to serve as the known loss-of-function mutant.[18] All variant cDNAs were confirmed by Sanger sequencing.

Immunofluorescence Microscopy

Mouse neuroblastoma 2A (N2A) cells were grown as previously described.[4] N2A cells on glass coverslips were transfected with 200 ng of plasmid DNA with the use of X-tremeGENE 9 DNA Transfection Reagent (Roche Diagnostics). After 24 hr, cells were fixed in PBS containing 4% paraformaldehyde for 15 min and permeabilized in PBS containing 0.1% Triton X-100 for 5 min. Cells were then blocked with 10% normal goat serum for 30 min. V5-tagged $G\alpha_{o1}$ was detected with a mouse V5 antibody (1:200 dilution; Life Technologies) and Alexa-488-conjugated goat anti-mouse IgG (1:1000 dilution; Life Technologies). Coverslips were mounted with Vectashield (Vector Laboratories) that contained DAPI and were visualized with an inverted FV1000-D confocal microscope (Olympus).

Structural Modeling and Free-Energy Calculations

We used FoldX software (version 3.0β5) to construct mutated molecular structures and calculate the free-energy changes caused by the mutations.[19] We used crystal structures of the GDP-bound inactive $G\alpha_i\beta\gamma$ heterotrimer (Protein Data Bank [PDB] 1GG2),[20] the nucleotide-free $G\alpha_s\beta\gamma$ in complex with agonist-occupied monomeric β2 adrenergic receptor (β2AR) (PDB 3SN6),[21] and the transition-state analog of GTP ($GDP^+AlF_4^-$)-bound $G\alpha_q$ in complex with its effector phospholipase C-β (PLCβ) (PDB 3OHM)[22] as three-dimensional structure models of the $G\alpha_o$ subunit in different complexed states. Each of the mutations, corresponding to p.Asp174Gly, p.Ile279Asn, or p.Gly203Arg in the human $G\alpha_o$ subunit, was introduced into the Gα subunit of each complex, and the free-energy change upon the mutation was calculated with FoldX software. Note that ligands included in the complexes were ignored in the calculation because the FoldX energy function

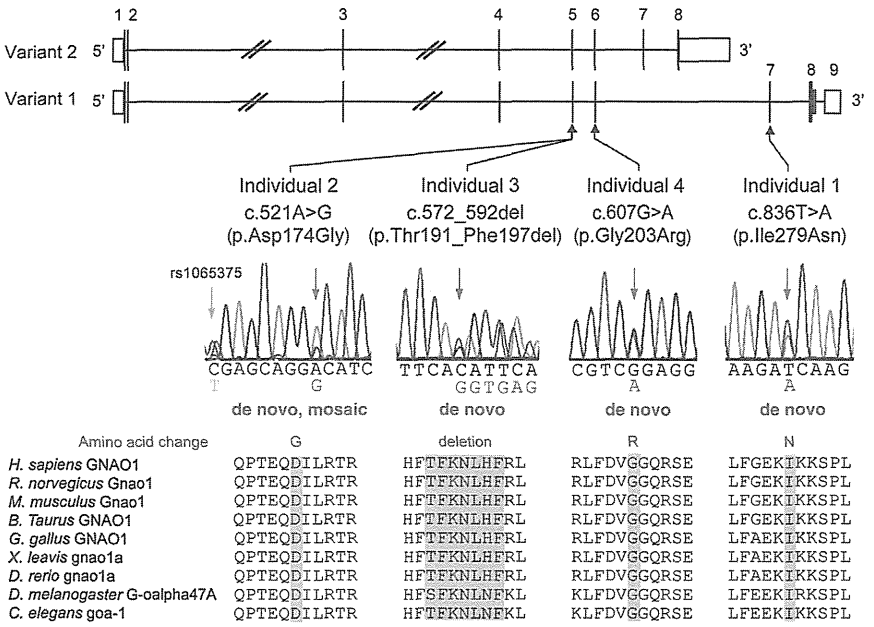

Figure 1. De Novo *GNAO1* Mutations in Individuals with Epileptic Encephalopathy
Schematic representation of *GNAO1*, including two transcript variants: transcript variant 1 (RefSeq NM_020988.2) with nine exons and transcript variant 2 (RefSeq NM_138736.2) with eight exons. The UTRs and coding regions are shown in white and black rectangles, respectively. Three mutations occurred in common exons of two transcript variants, and one mutation occurred uniquely in transcript variant 1. Note that the electropherogram of individual 2 suggested mosaicism of the c.521A>G mutation, and a heterozygous C>T change (rs1065375) was clearly demonstrated. All mutations caused substitution or deletion of evolutionarily conserved amino acids. Homologous sequences were aligned with the use of the CLUSTALW web site.

does not consider the contribution of ligands. The calculation was repeated three times, and the resultant data were presented as an average value with a SD.

Electrophysiology

For electrophysiological recording of calcium currents, we used NG108-15 cells transfected with individual *GNAO1* mutants. Expression vectors were introduced by electroporation with the Lonza Nucleofector device and the Cell Line Nucleofector Kit V (Lonza) according to the manufacture's protocol (program X-023). Two micrograms of plasmid DNA was used per transfection. The transfected cells were plated on poly-L-lysine-coated plastic coverslips (Cell Desk LF, MS-0113L; Sumitomo Bakelite) at a density of about 5×10^4 cells/cm^2 and cultured in Dulbecco's modified Eagle's medium (DMEM) supplemented with 10% fetal bovine serum (FBS). One day after transfection, the cells were differentiated with DMEM supplemented with 10 μM prostaglandin E1, 50 μM IBMX, and 1% FBS for 3–7 days before recording. During the culture period, half of the medium was changed every other day.

The recording was made by the perforated whole-cell patch-clamp technique with amphotericin B. Cells on coverslips were perfused under an Olympus BX51W upright microscope (Olympus) with a bath solution containing 140 mM NaCl, 5 mM $CaCl_2$, 4 mM KCl, 1 mM $MgCl_2$, 10 mM HEPES, 10 mM TEACl, 8 mM glucose, and 0.0002 mM tetrodotoxin (pH 7.3 adjusted with NaOH). The patch pipette solution contained 100 mM CsCl, 10 mM EGTA, and 40 mM HEPES (pH 7.3 adjusted with CsOH). Amphotericin B was added to the pipette solution at 2 μl/ml just before the experiments. The pipettes were fabricated from borosilicate glass capillaries and had a resistance of 4–8 MΩ when backfilled with the amphotericin-B-containing pipette solution. The recording was started when the series resistance was reduced to <150 MΩ after gigaseal formation and clear cellular capacitive surges had appeared. Voltage-gated calcium currents were elicited by the application of 50 ms depolarizing pulses to +10 mV from the holding potential of −65 mV, recorded with a Multiclamp 700B (Molecular Devices) controlled via pCLAMP10 software (Molecular Devices), filtered at 2 kHz, and sampled at 10 kHz with 50% compensation for series resistance. $G\alpha_o$-mediated current inhibition was elicited by the application of 10 μM norepinephrine via the bath solution. After 3–5 min, inhibition was assessed by measurement of the changes in current density just before the end of the depolarizing pulses. Recordings were made at room temperature.

Statistical multiple comparisons were made with ANOVA followed by Dunnett's post hoc test, and the threshold p value for judging statistical significance was 0.05. The current inhibition induced by norepinephrine in individual mutant-expressing cells was assessed with a paired t test. The results are given as the mean ± SEM.

Results

GNAO1 Is Mutated in Individuals with Epileptic Encephalopathy

We previously performed WES of 12 individuals with OS.[3,11] In this study, we analyzed parental samples from 5 of the 12 individuals by WES (mean RefSeq read depth of 109) to systematically screen de novo or recessive mutations. We found no recessive mutations in *SLC25A22* (MIM 609302), *PNPO* (MIM 610090), *PNKP* (MIM 613402), *PLCB1* (MIM 613722), or *ST3GAL3* (MIM 615006), whose mutations were previously found in epileptic encephalopathy,[23–27] but we did find one or two de novo mutations in each of the five trio exomes. Among them, a de novo missense mutation (c.836T>A [p.Ile279Asn]) in *GNAO1* at 16q12.2 was identified in individual 1. In the exome data of the other seven original individuals, we also found in individual 2 a second missense mutation (c.521A>G [p.Asp174Gly]), which was confirmed as a de novo event by Sanger sequencing (Figure 1). Moreover, *GNAO1* mutation screening in 367 individuals with epileptic encephalopathy by HRM analysis (339 individuals) and/or WES (100 individuals,